

A review of diaphragmless shock tubes for interdisciplinary applications

S. Janardhanraj*,¹ S. K. Karthick,² and A. Farooq¹

¹*Clean Combustion Research Center, King Abdullah University of Science and Technology, Thuwal 23955, Saudi Arabia^{a)}*

²*Currently at the Faculty of Aerospace Engineering, Technion - Israel Institute of Technology, Haifa 3200003, Israel*

(Dated: Received 2 December 2021; Received in revised form 18 September 2022; Accepted 25 September 2022)

Shock tubes have emerged as an effective tool for applications in various fields of research and technology. The conventional mode of shock tube operation employs a frangible diaphragm to generate shock waves. The last half-century has witnessed significant efforts to replace this diaphragm-bursting method with fast-acting valves. These diaphragmless methods have good repeatability, quick turnaround time between experiments, and produce a clean flow, free of diaphragm fragments, in contrast to the conventional diaphragm-type operation. The constantly evolving valve designs target shorter opening times for improved performance and efficiency. The present review is a compilation of the different diaphragmless shock tubes that have been conceptualized, developed, and implemented for various research endeavors. The discussions focus on essential factors, including the actuation mechanism, driver-driven configurations, valve opening time, shock formation distance, and operating pressure range, that ultimately influence the shock wave parameters obtained in the shock tube. A generalized mathematical model to study the behavior of these valves is developed. The advantages, limitations, and challenges in improving the performance of the valves are described. Finally, the present-day applications of diaphragmless shock tubes have been discussed, and their potential scope in expanding the frontiers of shock wave research and technology is presented.

CONTENTS

I. Introduction	2
II. Fast-acting valves in shock tubes	3
A. Wave system in a shock tube	3
B. Drawbacks of diaphragm-type shock tubes	5
III. Overview of fast-acting valve concepts	6
A. Early concepts (Prior to 1980)	6
B. Variants of Oguchi et al.'s double-piston design	7
C. Improvised designs for specific applications	8
D. Recent designs of fast acting valves (Post 2010)	9
IV. Design features of fast-acting valves	12
A. Closure element	12
B. Actuation and control elements	12
C. Driver-Driven configurations	14
1. Type-I driver-driven configurations	15
2. Type-II driver-driven configurations	16
3. Type-III driver-driven configurations	17
4. Type-IV driver-driven configurations	17
5. Type-V driver-driven configurations	17
V. Performance of fast-acting valves	17
A. Opening time of valve	17
B. Shock formation distance	19
C. Operating range, repetition rate and reliability	20
D. Performance in reflected shock mode	21

^{a)}Electronic mail: janardhanraj.subburaj@kaust.edu.sa

E. Improving valve performance	21
VI. Mathematical model for fast-acting valves	22
A. Case I: Annular driver configuration	
B. Case II: Inline driver configuration	23
VII. Shock wave applications using diaphragmless shock tubes: Current trends	26
A. Reliable studies in shock wave chemistry and physics	26
B. Exploring shock waves in miniature scales	27
C. Automating aerodynamic ground test facilities	28
D. Precise calibration of sensors	30
E. Novel industrial applications	31
F. Miscellaneous applications	31
VIII. Concluding remarks and future scope	32
Acknowledgments	32
References	32

I. INTRODUCTION

Shock waves are a fascinating physical phenomenon resulting from rapid compression in matter. They propagate at supersonic velocities, and their effects are observed in all forms of matter. The formation and propagation of shock waves in a gaseous medium are of particular interest in this review. A typical shock wave in gas is characterized by a moving shock front that increases the fluid's pressure, temperature, and density in a very short interval of time (referred to as the rise time of the shock wave). These thermodynamic properties remain constant for a period called the steady time and gradually decrease to the equilibrium state over the decay time. The rise time is typically on the order of microseconds. In contrast, the steady and decay times can range from microseconds to milliseconds depending on the energy of the source, method of shock wave production, and propagation dynamics. Shock waves are multi-scale and are observed in length scales varying from micro- to macroscopic regimes. This property has led to a plethora of shock wave-related disciplines being established for over a century now¹. The early applications of shock waves were in chemical kinetics and aerospace research to study processes in high-temperature gases and high-speed flows^{2,3}. The emerging applications of shock waves in interdisciplinary fields of science and technology have opened up new avenues for collaborative research⁴⁻⁶. Shock waves have also demonstrated the potential to address present-day industry challenges, such as preservative impregnation in bamboo, sandal oil extraction, removal of micron-size dust from silicon wafers, cell transformation, meat tenderization, and enhancing material properties⁷⁻¹⁰. The prospect of developing novel disruptive technologies using shock waves is an added incentive for modern technologists and entrepreneurs.

The sudden release of energy in a confined space results in a supersonic displacement of gas and leads to the formation of shock waves. Chemical, mechanical, nuclear, or elec-

trical energy can be a source of shock waves. Explosives¹¹, laser irradiation¹², electric discharge¹³, pressurized gases¹, and detonable gaseous mixtures¹ are commonly used to produce shock waves in gases for research purposes. Among these methods, the use of pressurized gas in a device called the shock tube¹⁴ is a simple, economical, and safe method to generate shock waves in a controlled manner. A simple shock tube comprises two sections separated by a diaphragm and is operated by pressurizing one section until the diaphragm ruptures to form a shock wave in the other section. Although shock tubes seem to have a simple operational procedure, the use of diaphragms has been found wanting for various reasons described in the following section. Therefore, a diaphragmless-mode of operation for shock tubes has been explored and implemented.

The main idea behind a diaphragmless shock tube is to eliminate the diaphragm burst process and replace it with a quick-opening valve while retaining the performance capabilities of a diaphragm-type shock tube. Ideally, a diaphragmless shock tube has good repeatability, a high repetition rate, the ability to automate, and requires less manual intervention and physical effort. Also, in a diaphragmless shock tube, the valve opening process does not contaminate the flow downstream, unlike conventional diaphragm-type shock tubes. The opening time in the case of a diaphragm rupture generally varies from hundreds of microseconds to a few milliseconds depending on the diameter, pressure difference, material properties, and thickness of the diaphragm. Practically, it is an engineering and manufacturing challenge to design fast-acting valves with large diameters and opening times on the order of milliseconds. Moreover, producing a high-enthalpy shock wave using a diaphragmless valve as required in certain aerodynamic testing facilities^{15,16} and materials research^{17,18} is even more cumbersome. Numerous diaphragmless valve concepts have been proposed since the first concept of a 'shock wave valve' was introduced by Condit in 1954¹⁹. With advances

in manufacturing technology and high-performance actuation systems, fast-acting valves with improved performance and efficiency have been realized.

An assessment of diaphragmless shock tubes has been reported previously^{20–22}, but the review was limited to only a few design concepts. The present work is a comprehensive compilation of diaphragmless valve concepts reported for over half a century, and it is the first such review to the best of our knowledge. The basic parameters and terminology used in diaphragmless shock tubes are initially defined and elucidated. Subsequently, the different design concepts reported in the literature are distinguished based on the mounting configuration, operating principle, and actuation mechanism. The advantages and shortcomings of specific diaphragmless valve designs have been identified. A generalized mathematical model and relations for opening time are presented based on the typical forces experienced by the moving element in a diaphragmless valve. A detailed procedure of the various design points that must be considered while developing such valve concepts has also been included, which helps analyze the valve performance analytically. The modern applications of shock waves that have unfolded with diaphragmless shock tubes in various fields of research and technology have been reviewed. Overall, the present communication attempts to identify the gaps, challenges, and opportunities in developing diaphragmless valves for interdisciplinary shock wave applications.

II. FAST-ACTING VALVES IN SHOCK TUBES

The wave systems in a diaphragm-type and a diaphragmless shock tube are discussed considering a simple 1-D inviscid adiabatic flow. The use of diaphragms in a shock tube comes with numerous disadvantages. The major shortcomings of conventional shock tubes and how these are addressed using fast-acting valves are also described in this section.

A. Wave system in a shock tube

The flow field in a shock tube is complex, unsteady, and dependent on the initial conditions in the two sections of the shock tube. Generally, the pressurized gas filled in the high-pressure section of the shock tube is termed the “driver gas,” while the gas filled in the low-pressure section is called the “test gas” or “driven gas.” When the barrier between the driver and driven gas is removed, a shock wave is formed that propagates in the low-pressure section. Simultaneously, expansion or rarefaction waves propagate in the opposite direction into the high-pressure chamber. The expansion fan region gradually reduces the pressure and temperature of the driver gas and is bound by the rarefaction head and tail. The rarefaction waves get reflected from the end-wall of the high-pressure section and then travel towards the driven gas region. Meanwhile, the shock wave travels towards the end-wall of the low-pressure section, where the incident shock wave compresses the gas behind it. The incident shock wave reflects off the end wall and travels into the onward flow, increasing the pressure

and temperature a second time. For studies that utilize the incident shock wave, the steady time of the shock wave at a given location is the time interval between the arrival of the shock front and the contact surface (an imaginary surface that separates driven and driver gases). Most of the studies utilize the stationary shocked gas behind the reflected shock. In this case, the steady time window is the time interval between the reflection of the incident shock wave and the reflected waves from the contact surface.

The entire flow in the shock tube is generally divided into five regions. Region 1 and 4 are the undisturbed gas in the shock tube’s low- and high-pressure sections, respectively. Region 2 represents the gas between the incident shock wave and the contact surface, while region 3 is the flow behind the contact surface. The stagnant gas behind the reflected shock wave is in region 5. Thermodynamic parameters in these regions are indicated by using the corresponding number of the region as a subscript. For example, P_4 and T_4 are the pressure and temperature of the undisturbed driver gas, while P_1 and T_1 represent the pressure and temperature of the undisturbed driven gas, respectively. The ratio between the parameters in different regions is also generally represented using a subscript. For example, the ratio of P_4 and P_1 is indicated as P_{41} , ratio of T_4 and T_1 as T_{41} and so on. The relationship between the initial conditions and the shock wave parameters can be solved exactly for a simple case assuming a one-dimensional, inviscid, and adiabatic flow³. The pressure ratio, P_{41} , is related to the shock Mach number, M_S , as,

$$P_{41} = \frac{2\gamma M_S^2 - (\gamma - 1)}{\gamma + 1} \left(1 - \frac{\gamma - 1}{\gamma + 1} \frac{a_1}{a_4} \left(M_S - \frac{1}{M_S} \right) \right)^{-\frac{2\gamma}{\gamma - 1}} \quad (1)$$

where γ is the specific heat ratio and a is the local speed of sound. A helpful method to represent the wave system in a shock tube is using an $x-t$ diagram or wave diagram. This diagram is constructed using a technique called the method of characteristics that considers flow perturbations to travel at the local speed of sound. For a stationary observer, the perturbations inside the shock tube travel with the sum of the local speed of sound and the gas velocity. It is also assumed that the shock wave instantly forms at the diaphragm location after the rupture. The wave diagram for a diaphragm-type shock tube is commonly used and can be found in multiple references^{2,3}.

The flow in a diaphragmless shock tube can also be represented using an $x-t$ diagram, assuming one-dimensional, inviscid, and adiabatic flow. Here, since a fast-acting valve replaces the diaphragm at the interface between the driver and the driven gas, the slower opening of the valve compared to the diaphragm rupture time results in a longer shock formation distance. Hence, the shock formation in a diaphragmless shock tube is an important process that has to be shown in the wave diagram. To understand the growth of the shock wave as a result of the finite opening time of the valve, the accelerating piston analogy described by Becker is useful²⁴. Consider a tube inside which a piston accelerates from rest to a constant velocity, v (v greater than the speed of sound). Let the piston reach velocity v through small increments over a fi-

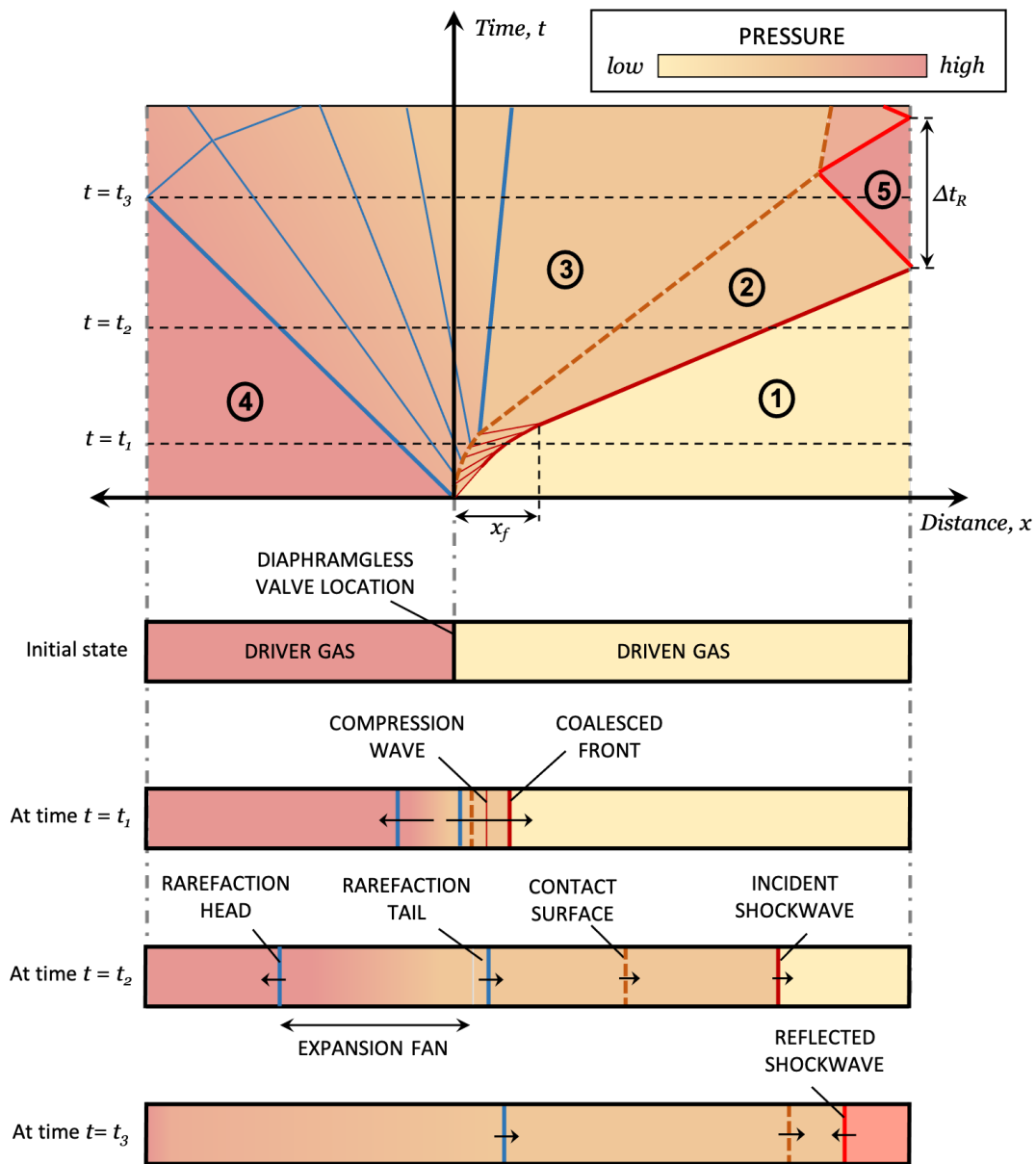


FIGURE 1. A schematic diagram showing the distance-time ($x-t$) plot along with pressure contour for a diaphragmless shock tube and the corresponding wave system at time instants $t = 0$, $t = t_1$, $t = t_2$ and $t = t_3$. x_f indicates the shock formation distance and Δt_R is the steady time of the reflected shock wave. (Adapted by permission from The Japan Society of Mechanical Engineers: Bulletin of JSME, Ikui et al.²³, copyright 1979)

nite time. The first increment in piston velocity causes a weak compression wave to propagate in the tube, compressing the gas uniformly and adiabatically behind it. The compression wave generated by the second velocity increment travels in a gas with a slightly higher sound speed due to the preceding compression wave's propagation. Subsequently, each compression wave produced by the piston motion moves in a gas, pressurized and heated by the previous compression wave, and eventually catch up with the preceding waves. The waves coalesce to form a shock wave that reaches a steady velocity when the piston's speed becomes steady. In a shock tube, the

motion of the piston is analogous to the contact surface, which is a constant-pressure interface.

Figure 1 shows the wave diagram for a diaphragmless shock tube with a pressure contour to highlight the typical pressure variations in the tube. The position of the corresponding waves in the shock tube at different time instants ($t = 0$, $t = t_1$, $t = t_2$ and $t = t_3$) are shown below the wave diagram. The initial state of the shock tube is shown at time $t = 0$. At the time $t = t_1$, the shock wave formation from compression waves is seen. The fully developed flow in the diaphragmless shock tube is seen at $t = t_2$. The reflections of the shock wave

and expansion waves from their corresponding end-walls are seen at time $t = t_3$. The steady time duration in the reflected shock region is represented by Δt_R . Figure 1 also shows the development of the coalesced shock front from the merging of the characteristics developed due to the accelerating contact surface²⁵. The distance from the initial driver-driven gas interface to the location where the shock wave is formed is termed as the shock formation distance (x_f). The shock formation distance is also the distance from the driver-driven interface where the shock front reaches the maximum velocity. The shock formation process in the shock tube is directly proportional to the opening time of the shock tube. The slower the opening time of the valve, the longer the shock formation distance²⁶. Therefore, diaphragmless shock tubes need longer driven sections, in general, compared to conventional diaphragm-type shock tubes.

B. Drawbacks of diaphragm-type shock tubes

The major reasons for exploring alternatives to conventional diaphragm-type shock tubes are listed below:

- **Run-to-run variation** - The ability to replicate the burst process of the diaphragm determines the reproducibility of the shock wave conditions in the shock tube. The diaphragm opening can be very irregular, and, on many occasions, a part of the diaphragm can obstruct the flow of gas due to an incomplete opening^{27,28}. Therefore, every experiment performed in a diaphragm-type shock tube has a unique flow condition as the burst process differs for every run. The inability to obtain repeatable test conditions is a significant drawback of diaphragm-type shock tubes.
- **Long turnaround times** - Diaphragm replacement is time-consuming in many shock tube facilities. In most cases, it might take a few minutes or even an hour in some large facilities. For investigations requiring shock waves to be produced at a high repetition rate (on the order of seconds or lower), the conventional diaphragm-type shock tube is unsuitable.
- **Manual effort** - Large-scale shock tubes typically have lengths of about 10–15 m and internal diameters in the range of 50–200 mm. There is a requirement for sufficient human resources or, in some cases, expensive hydraulic systems to disassemble bulky flanges at the diaphragm stations. In the case of miniature shock tubes, diaphragm changing becomes very cumbersome because of small-size fasteners. Also, manual effort is required to employ the best quality control methods in diaphragm manufacturing. Eliminating manual intervention is necessary to automate the shock tube facility. Automation can help shift the focus from spending time/energy operating the shock tube to the primary research/project goals.
- **Debris from diaphragm rupture** - The diaphragm rupture is a source of tiny fragments carried by the flow to the end of the shock tube. This debris produced by diaphragm rupture is particularly menacing for test samples, sensors, observation windows, and diagnostics in the shock tube. The fragments accumulate in the shock tube after several experiments and must be removed to avoid further damage to components in pneumatic lines. In some specific chemical kinetic studies, it has been observed that the debris can cause inhomogeneous ignition of fuels and hence lead to undesirable effects²⁹. The process of removal of debris and cleaning the shock tube is cumbersome and time-consuming.
- **Unique opening time in every experiment** - Although instantaneous removal of the diaphragm is quintessential in an ideal shock tube, in reality, the diaphragm rupture process takes a finite time. The complex flow phenomena generated close to the diaphragm location depend on the diaphragm's opening time, which in turn is strongly related to the diaphragm's material properties of the diaphragm^{30,31}. Different materials (polycarbonate, steel, aluminum, Mylar, Lexan, etc.) of varying thicknesses are used as diaphragms to vary the shock wave conditions. Therefore, the opening time of the diaphragm is unique for a particular combination of the diaphragm material, thickness, and shock tube dimensions³².
- **Resistance behavior of thicker diaphragms** - In high-pressure shock tubes, thicker diaphragms have to be used to produce strong shock waves. It has been reported that thicker diaphragms exhibit significant resistance to opening due to the stresses at the hinge line of the diaphragm³³. Therefore, the flow produced in high-pressure shock tubes depends on thicker diaphragms' resistance behavior.
- **Extremely thin diaphragms for small shock tubes** - Engineering a small-scale shock tube poses many challenges as the diaphragm thickness would be on the order of micrometers or nanometers³⁴. A very minute change in the thickness of the diaphragm is required to vary the burst pressure in small steps. In practice, it would be challenging and expensive to fabricate such diaphragms. Therefore, an alternative to using diaphragms is necessary for miniature shock tubes. For low-pressure applications, the flow behind the incident shock wave can be used instead of the conditions behind the reflected shock wave, depending on the nature of the experimental study. Nevertheless, the diaphragm choice for small increments in the burst pressure remains.
- **Consumable and waste footprint** - Diaphragm-type shock tubes require the replacement of the frangible diaphragm after every single run. There is significant wastage of material during the fabrication of diaphragms and after the completion of experiments.
- **Impurities in ambient air** - In diaphragm-type shock tubes, an inert gas is filled in the tube when changing a

diaphragm to avoid the release of harmful gases from previous experiments to be released into the ambient air. There are a few specific applications, such as in Gas Dynamic Lasers (GDL), for which it is essential to avoid the exposure of the inside of the shock tube to ambient air after every test³⁵. Certain species in the ambient air can act as impurities and excite/de-excite the upper/lower laser levels. In such applications, a diaphragmless shock tube is a safer option.

Several methods have been reported to minimize shot-to-shot variation in diaphragm rupture. Generally, a V-groove notch is machined along two diameters at right angles to form a cross-shape (×) on the exposed portion of the diaphragm facing the low-pressure section³. The high-pressure fractures the diaphragm along the preferential cross-shape and opens into the low-pressure section with the formation of four petals. Using electrical discharge to initiate diaphragm breaking gives short opening times and precise timing of the rupture^{36,37}. A diaphragm-cutter can also obtain controlled diaphragm bursts, as demonstrated in a 432 mm diameter shock tube, to get an opening time of about one millisecond³⁸. The diaphragm bulges after pressurizing the high-pressure section, and the cutter is optimally placed so that the diaphragm is cut into four sections that open out like petals. A gas-operated clamp with a needle has also been reported to obtain repeatable diaphragm bursts and quick changing of the diaphragm (≤ 1 min)³⁹. Another novel method is using a double-diaphragm technique which is commonplace in high-pressure shock tubes, especially while avoiding the use of thicker diaphragms⁴⁰. By quickly evacuating a small buffer volume between the two diaphragms, the rupture of the two diaphragms is attained at the required pressure. These techniques work reasonably well in addressing run-to-run variations, but the other drawbacks of using diaphragms need to be tackled.

III. OVERVIEW OF FAST-ACTING VALVE CONCEPTS

Numerous diaphragmless valves with different configurations have been designed and implemented for research and technological applications. Each design has unique features in terms of operating principle, actuation techniques, mounting configuration, operating pressure range, overall size, and shock tube dimensions, making these suitable for the specific studies they facilitated. Diaphragmless valve designs are analyzed based on these features in the following sections.

A. Early concepts (Prior to 1980)

Condit¹⁹ presented the idea of a shock wave valve that consisted of a piston held in position by pressurizing gas in an actuating chamber behind it (described in Muirhead et al.⁴¹). The design incorporated an annular driver section and a cam-actuated poppet, which quickly released the gas in the actuating chamber, allowing rapid retraction of the piston that initially sealed the driver gas. Condit's design was implemented

in shock tubes with driven section diameters of 1 in. and 17 in. for maximum driver pressures of 600 and 200 psi, respectively. Muirhead et al.⁴¹ modified Condit's design by replacing the poppet with an auxiliary piston that releases only a portion of the gas behind the main piston (see Fig 2). The remaining gas was used to bring the main piston back to the original position to control the positive duration of the shock wave. They also suggested a concept for higher driver pressures (up to 2000 psi) in which the piston had a smaller exposed area, and the driver section was placed in line with the driven section. Oguchi et al.⁴² replaced the cam-release mechanism with a solenoid valve for quick action. Their design primarily consisted of a smaller auxiliary piston to control a larger main piston's motion. The solenoid valve releases a small volume of high-pressure gas behind the auxiliary piston to produce quicker retraction of the main piston. In this design, the size of the main piston was comparable to that of the driven section (smaller piston size compared to Condit's and Muirhead et al.'s designs). Shock Mach numbers of about 4.1 were obtained using this design, and many researchers widely used the solenoid-actuated double-sliding piston arrangement for future studies. Distefano et al.⁴³ suggested an electromagnetically operated diaphragmless valve that utilizes two coils, one fixed and the other sliding, fixed to plates. When current flows through the coils, the seal plate slides into place and seals the driver section. When there is a sudden pressure increase due to combustion in the driver section or a short current interruption, the seal plate retracts and produces a shock wave.

Garen et al.⁴⁷ used a rubber membrane to seal the driven section from the driver section. The rubber membrane was inflated, by pressurizing a volume behind it, to block the entry into the low-pressure chamber. The bursting of a secondary diaphragm released the pressure behind the membrane. The retraction of the membrane led to the formation of shock waves in the driven section. This mechanism was used in a shock tube with an 18 mm square driven section and a 36 mm circular driven section. The replacement of the secondary diaphragm after every run and restriction to low driver pressures were significant drawbacks of this design. Matsuo et al.⁴⁸ suggested that the vertical movement of the piston was ideal for replacing the diaphragm in shock tubes. The low operating range of driver pressure (≤ 1 bar) was a significant shortfall of these designs. Oguchi et al.⁴⁴, and Ikui et al.⁴⁵ presented a novel and sophisticated design for fast-acting pistons, which could be mounted inline with the driver and driven sections of a 100 mm by 180 mm diaphragmless shock tube (described in details in other reports^{46,49,50}). Therefore, there was no major redirection of gas flow from the driver to the driven section, as seen in Figure 3. The piston was accelerated into a teardrop-shaped coaxial section by venting the chamber behind it due to an auxiliary diaphragm rupture. A spring mechanism assisted this motion. A spring and gas damper was utilized to prevent piston damage due to impact and also helped bring the piston back to its original position. The valve produced shock Mach numbers in the range of 1.2-5, and the shock formation length was about 50 tube diameters. A clearance distance was incorporated to obtain an immediate opening of the

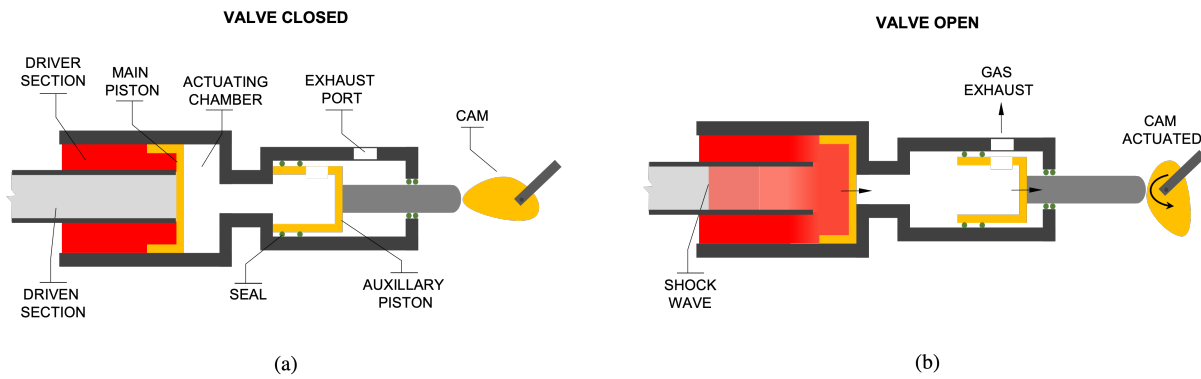


FIGURE 2. Schematic diagrams showing the valve design proposed by Muirhead et al.⁴¹ (Adapted by permission from AIP Publishing: Review of Scientific Instruments, J. C. Muirhead and W. A. Jones⁴¹, copyright 1964). A double piston arrangement was used in a coaxial driver-driven configuration actuated using a cam. (a) Valve in the closed position with the high-pressure driver gas filled in the driver section. (b) The valve opens when the cam is actuated, retracting the main and auxiliary piston. Cam was replaced by a solenoid valve by Oguchi et al.⁴²

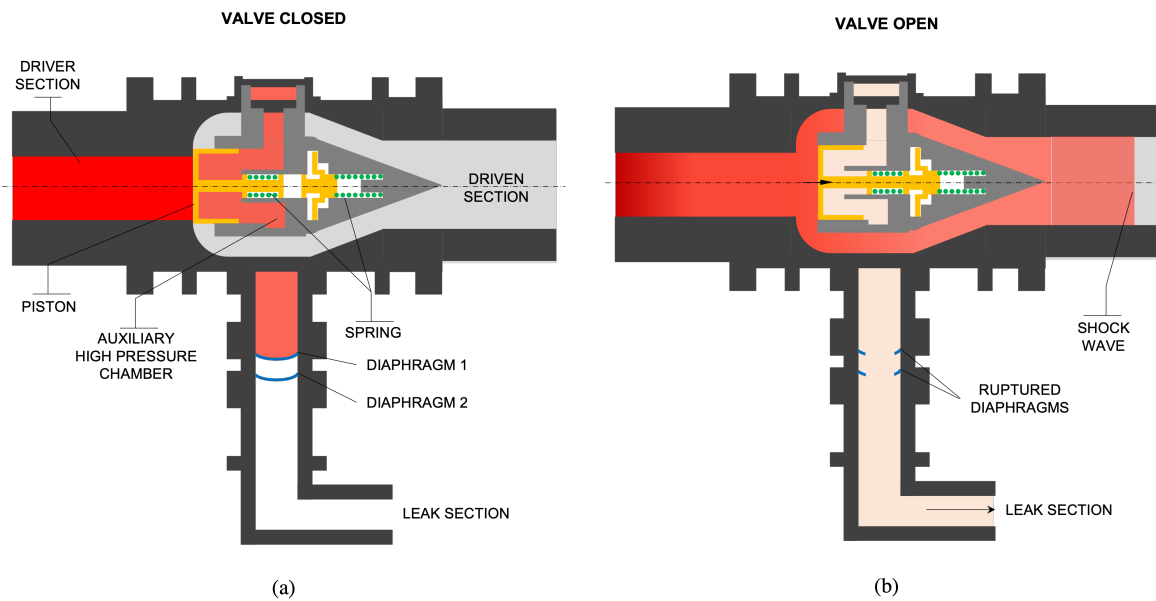


FIGURE 3. Schematic diagrams of the valve designed by Oguchi et al.⁴⁴ and Ikui et al.⁴⁵. Driver and driven sections are mounted inline and piston accelerates into a teardrop-shaped coaxial section. (a) When the valve is closed, the piston is held in place by high-pressure in an auxiliary chamber by means of diaphragms. (b) The valve opens when the diaphragms are ruptured and the high-pressure auxiliary chamber is evacuated, retracting the piston. (Adapted by permission from Springer Nature: Experimental Methods of Shock Wave Research by Igra, O., Seiler, F.⁴⁶, copyright 2016)

valve in the piston-based valves in Ikui et al.'s designs²⁵. The piston accelerated and traversed the clearance distance before it breached the seal between the driver and the driven section. They designed a valve that opens along the shock tube axis, a double-piston sliding arrangement, and electromagnets for actuation. Since the piston moves horizontally, they called it a type-H valve. They also described a valve that opens perpendicular to the shock tube axis (called a type-V valve because of the vertical motion of the piston), which required the piston to move a more considerable distance than the type-H valve.

In both cases, the valve's performance depended on the pressures in the actuating and driver chambers. The opening time and shock formation distance of the type-H valve were investigated at different pressures in the chambers²³.

B. Variants of Oguchi et al.'s double-piston design

Oguchi et al.'s design principle was used in a shock tube for experiments in low-temperature gases⁵¹ (as low as 150 K)

and gas dynamic laser applications^{52,53}. The low temperatures were obtained by cooling the driven section with liquid nitrogen⁵¹. The snap-action shock tube had a main and auxiliary piston made of nylon and actuated using electromagnetic valves. The maximum driver pressure was 5 bar, and the driven section had an inner diameter of 19.4 mm. Maeno and Oguchi⁵⁴ performed studies using the synchronized operation of two diaphragmless shock tubes (with internal diameters of 20 mm and 50 mm) that implemented the double-piston arrangement actuated by electromagnetic valves. Solenoid valves helped time the actuation precisely to obtain the required delay in shock wave generation. A modified piston-driven shock tube actuated by solenoid valves and having a similar arrangement to Oguchi et al.'s design was also reported by Yamauchi and coworkers⁵⁵. This design implemented the main piston made of aluminum and a nylon auxiliary piston. Driver pressures of up to 20 bar were used in the shock tube with a 30 mm driven tube diameter. Hurst et al.⁵⁶ adopted Yamauchi et al.'s design to develop an enlarged version of the double-piston arrangement. They significantly shortened the turn-around time between runs by automating the facility and showed good repeatability. The principle of Oguchi et al.'s design, with minor modifications in the supply of pressure, was used by Matsui et al.⁵⁷ to obtain good reproducibility in shock wave conditions at low operating pressures with a temperature scatter behind the reflected shock as low as ± 20 K. Takano et al.⁵⁸ demonstrated a lightweight piston arrangement that was operated by magnetic valves and the system required little time for the initial setup to run the shock tube. The maximum driver pressure was 9 bar, and the design employed an annular driver-driven configuration. They also incorporated a lip in the piston to accelerate before breaching the seal between the driver and driven sections.

A vertical shock tube system implementing the double-piston arrangement actuated by magnetic valves was reported by Teshima⁵⁹. In this design, an annular driver section was used, and the generated shock wave traveled vertically down in the driven section. shock waves with Mach numbers up to 2 were generated with a high-repetition-rate in a 16 mm diameter driven tube. The double-piston actuated design was further developed and implemented by Rego et al. in their large diameter diaphragmless shock tube^{35,60}. Improvements were suggested in the choice of piston material, seals, piston shape, and damping element to achieve good cycle life of operation. Onodera⁶¹ improved the double-sliding piston design of Oguchi et al. by combining the functions of the auxiliary and main piston into a more complex single composite piston. The composite piston had a large front end that sealed entry to the driven section and a smaller back end connected through a stem. The high-pressure gas in the small volume behind the piston, which initially keeps the piston in place, was rapidly exhausted by a solenoid valve. The gas surrounding the piston stem was evacuated to ensure minimum resistance to the piston movement. The complex geometry of the piston, the intricate sealing requirements, and the considerable weight of the piston were some disadvantages of this design. The small exhaust volume in the design helped achieve quick retraction to produce shock waves with a Mach number of 1.2. Mejia-

Alvarez et al.²¹ developed a sophisticated design for a double-sliding piston vertical shock tube based on a one-dimensional compressible flow model. This design had an annular driver section with many unique features that helped it outperform previous similar configurations. They analyzed all the variants of Oguchi et al.'s design before optimizing their structure. Figure 4 shows the different possible moving elements used in Oguchi et al.'s concept. They also highlighted the crucial role of the discharge orifice in providing the quick retraction motion of the piston. A diaphragmless driver using a double-sliding piston arrangement was also reported for studies in a 19.4 mm diameter driven tube⁶².

C. Improvised designs for specific applications

Kosing et al.²⁰ used an annular driver section with a single large piston while introducing a new actuation mechanism that did not utilize an auxiliary pressure chamber. The chamber behind the piston was evacuated to prevent the retraction movement, and the driver gas pressure aided the piston's acceleration. A steel brake pad mechanism on the piston side was installed to provide enough frictional force to hold the piston in place, which helps seal the driven section. The brake pad was operated using a hydraulic actuator with a small pressurized reservoir to provide sufficient force to hold the brake pad in place. Since the hydraulic fluid is incompressible, the pressure drop in the reservoir was very rapid, and the frictional force holding the piston dropped to zero. Different piston materials were experimented with, and the system produced a good performance for shock Mach numbers up to 2. A vertical co-axial shock tube with the double-piston arrangement was developed to generate toroidal shock waves traveling upwards in the driven section⁶³. The pistons were ring-shaped and relatively heavy, resulting in slower opening times and a more considerable formation distance. A vertical diaphragmless shock tube with a 60 mm by 150 mm low-pressure channel was also developed. This facility was used to quantitatively visualize shock waves in a holographic interferometric system^{5,6,64}. Miyachi et al.⁶⁵ proposed two piston-driven diaphragmless shock tubes; the first design used five neodymium magnets for actuation, while the second valve was actuated electropneumatically to release the gas from a pressurized chamber behind the piston. Both designs incorporated a clearance distance in the piston movement for quicker opening. These designs were demonstrated in a 10 mm diameter shock tube for up to 8 bar driver pressures.

A rapid opening valve assisted by magnetic force was used in a diaphragmless shock tube with a 10 mm internal diameter⁶⁶. The axis of the driver and the driven sections were perpendicular to each other, and the maximum driver pressure used was 9 bar. Abe et al.⁶⁷ developed a high-speed valve to replace the use of diaphragms in a free-piston shock tube. Conventionally, the diaphragm in a free-piston shock tube ruptures when a piston moves towards it, accelerated by high-pressure gas from a reservoir and compresses the gas ahead. Abe et al. designed a valve with two-piston cylinders that moved perpendicular to the axis of the shock tube. An electro-

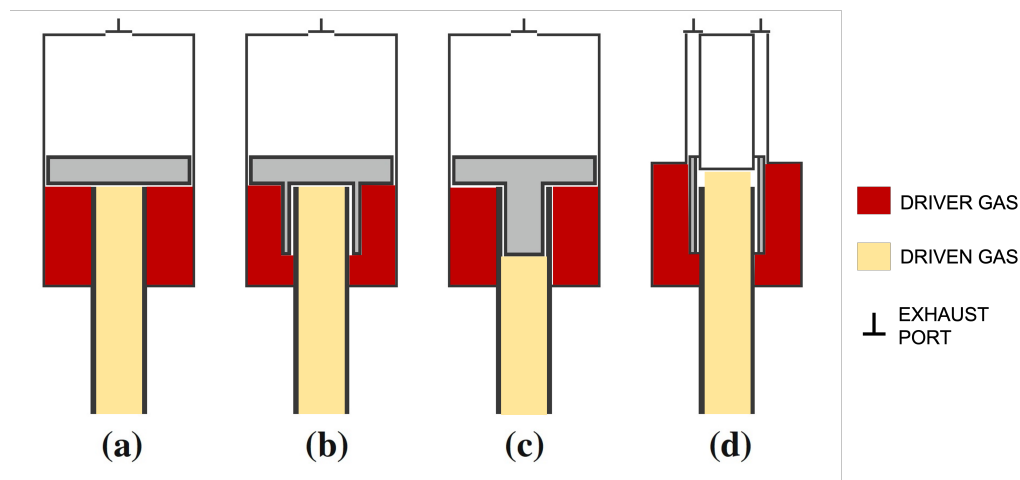


FIGURE 4. Variants of Oguchi et al.'s design as suggested by Mejia-Alvarez et al.²¹ (a) Piston, (b) Piston with lip, (c) Piston with plug, and (d) Sleeve-type. (Adapted by permission from Springer Nature: Shock Waves, Mejia-Alvarez et al.²¹, copyright 2015)

magnetic valve that released the high-pressure gas to drive the free piston actuated the entire facility. The fast-acting valve operates automatically when the free piston compresses the gas. Bredin and Skews⁶⁸ used a three-piston configuration valve in a 50-meter long diaphragmless shock tube in which the opening times of the valve could be varied to obtain compression waves with rise times in the range of 5 to 20 milliseconds. The main piston was actuated using a secondary piston, and a tertiary piston was used to provide forward motion for the secondary piston. The use of multiple pistons made the operation of the shock tube very complicated. Another study compared a diaphragmless shock tube operated by a double-acting pneumatic cylinder and using a membrane-based fast-acting valve⁶⁹. The valve opening speed of the pneumatic-cylinder-based valve varied from 0.325 to 1.15 m/s, while it was around 8.3 m/s for the membrane-based valve. Shock Mach numbers of up to 2.125 were obtained with good repeatability using the double-acting pneumatic cylinder-based valve. A valve similar to that reported by Oguchi et al.⁴⁴ and Ikui et al.⁴⁵ consisting of a piston, spring dumper, and piston driver was operated using either a small diaphragm or a solenoid valve^{70,71}. Itahashi et al.⁷² optimized the opening of the driver gas to the driven section, thus resulting in a more efficient driver than most previous designs.

Garen et al.'s design⁴⁷ was implemented in a 1 mm driven tube made of glass to study shock wave phenomena in miniature scales^{75,76}. The propagation velocities of the shock waves were measured with a specially designed laser interferometer, and experiments were performed up to driver pressures of 2 bar. The investigations were also extended using the same diaphragmless driver in a 3 mm driven tube, and the motion analysis of the rubber membrane was performed to evaluate the performance of the valve^{77,78}. Another membrane-based design with repeatability of 99 % for shock Mach numbers in the range of 1.02-1.55 was proposed⁷³. Support blocks and grids were provided to limit the displacement of the rubber sheet and eliminate the expansion waves due to the rapid movement of the rubber sheet (see Fig 5). The piston-based

design⁶³ to generate toroidal shock waves was improved by using a re-usable rubber membrane in a vertical shock tube⁷⁹. Perforated ring-shaped steel plates were used to limit the rubber membrane's motion and to ensure the deformation was within the elastic limits. Consistent operation and a high degree of repeatability were ensured utilizing this technique, although the maximum shock Mach number was limited to 1.8⁸⁰. A bellow-actuated diaphragmless valve was used to obtain reasonable control over the opening and closing of the valve⁸¹. Bellows were pressurized to provide a forward motion to seal the driven section from the annular driver section. The sudden release of the gas inside the bellows rapidly opened the pathway between the driver and the driven chamber. An alternative design based on Kim's design⁸¹ was presented⁷⁴, as shown in Figure 6. The problem of vibrations and alignment during the operation was minimized in the 71 mm internal diameter shock tube using linear bearings to support the bellow-piston arrangement. The design showed good shot-to-shot reproducibility over a range of operating conditions. An improved driver design was later suggested⁸² where the bellow is placed in a manner such that it is compressed rather than extended when the driver gas is filled. With the growing interest in miniature shock wave applications, significant efforts were made to build small-scale high-repetition-rate automated shock tube systems. Shiozaki et al.⁸³ built a 2 mm internal diameter diaphragmless shock tube that generated shock waves with Mach numbers of up to 2.8 and a temperature behind the reflected shock of about 1200 K. The solenoid-operated poppet valve produced high-repetition-rate shock waves at 5 Hz.

D. Recent designs of fast acting valves (Post 2010)

In contrast to previous designs, Heufer et al.⁸⁴ suggested a sleeve-type fast-acting valve in which the driver and driven sections have the same cross-section area and are mounted in line with each other (see Fig 7). Shock Mach numbers

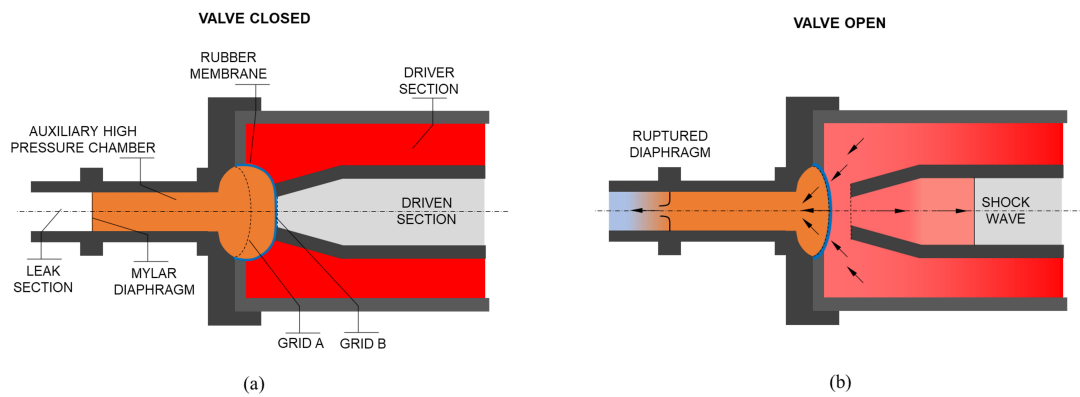


FIGURE 5. Fast-acting valve utilizing a rubber membrane proposed by Yang et al.⁷³ (a) Valve is closed: The rubber membrane bulges and blocks the path between the driver and driven section when an auxiliary chamber is pressurized. (b) Valve is open: When a diaphragm holding the pressurized gas in the auxiliary chamber is ruptured, the membrane retracts and opens the driver volume to the driven section. (Adapted with permission from The Japan Society of Mechanical Engineers: Transactions of the Japan Society of Mechanical Engineers Series B, Yang et al.⁷³, copyright 1994)

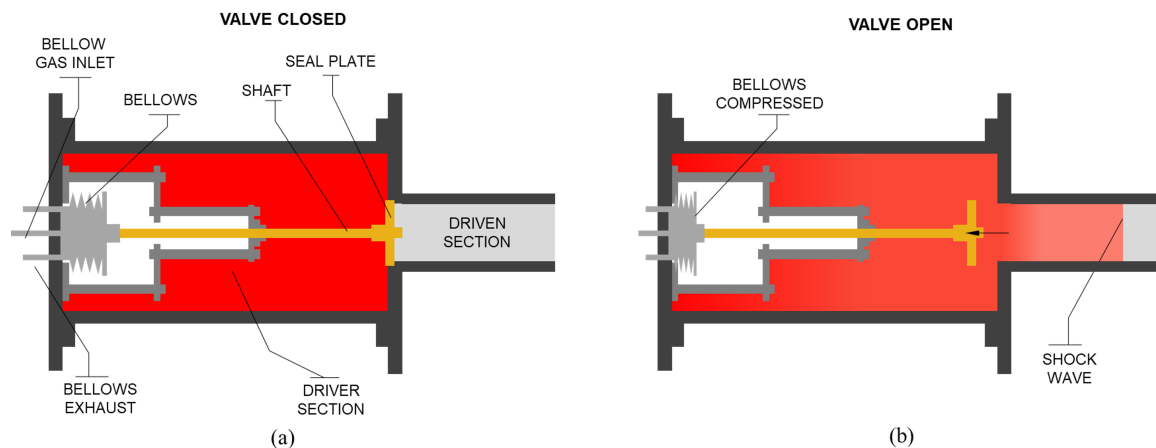


FIGURE 6. Fast-acting valve design used by Tranter et al.⁷⁴ that incorporated bellows for quick retraction of the piston. Different variations of this arrangement have been later designed by researchers. (a) A long shaft attached to the bellow moves forward to block the driver section from the driven section. (b) The piston retracts due to the bellow action to open the path between the driver and driven section. (Adapted with permission from AIP Publishing: Review of Scientific Instruments, Tranter et al.⁷⁴, copyright 2008)

of up to 3.4 were obtained for driver pressures of 30 bar. Downey et al.⁸⁵ introduced a fast-opening valve that uses a sleeve to block the driver gas from entering the driven section initially. They incorporated multiple new features that improved the operating pressure range of the valve (up to 200 bar) while achieving short opening times. The sleeve also had a lip similar to Takano et al.'s design⁵⁸ for faster opening times. The sleeve was made of aluminum alloy, and the annular driver section had a streamlined flow path to minimize losses. The double-piston arrangement was adopted for studies in a miniature shock tube⁸⁶ as well with the development of a valve called the Maeno-Oguchi valve (described in Udagawa et al.⁸⁷). This valve was used for studies in a miniature 2 mm and 3 mm internal diameter shock tube with driver pressures up to 9 bar. An improved version called the Udagawa-Maeno-Oguchi valve was also reported that used a clearance

distance for piston movement that helped in faster retraction speeds and smaller opening times⁸⁷. Based on the Tranter et al.'s bellow valve design⁷⁴, a new diaphragmless shock tube, called the Brown Shock Tube (BST), with software control and actuation of valving was presented⁸⁸. The operating pressures were increased up to 100 bar in the diaphragmless shock tube with a driven section diameter of 100 mm. McGivern et al.²² used a piston that was connected directly to the movable end of fixed stainless steel bellows for low-pressure application. This design incorporated a plug instead of a flat piston so that the piston accelerates before breaching the seal.

A 6.35 mm bore diaphragmless shock tube called the high repetition rate shock tube (HRRST) was designed for operational pressures up to 100 bar and observation times of about 100 microseconds⁹⁰. This diaphragmless driver was actuated using a solenoid valve, had a cycle rate of up to 4 Hz, and was

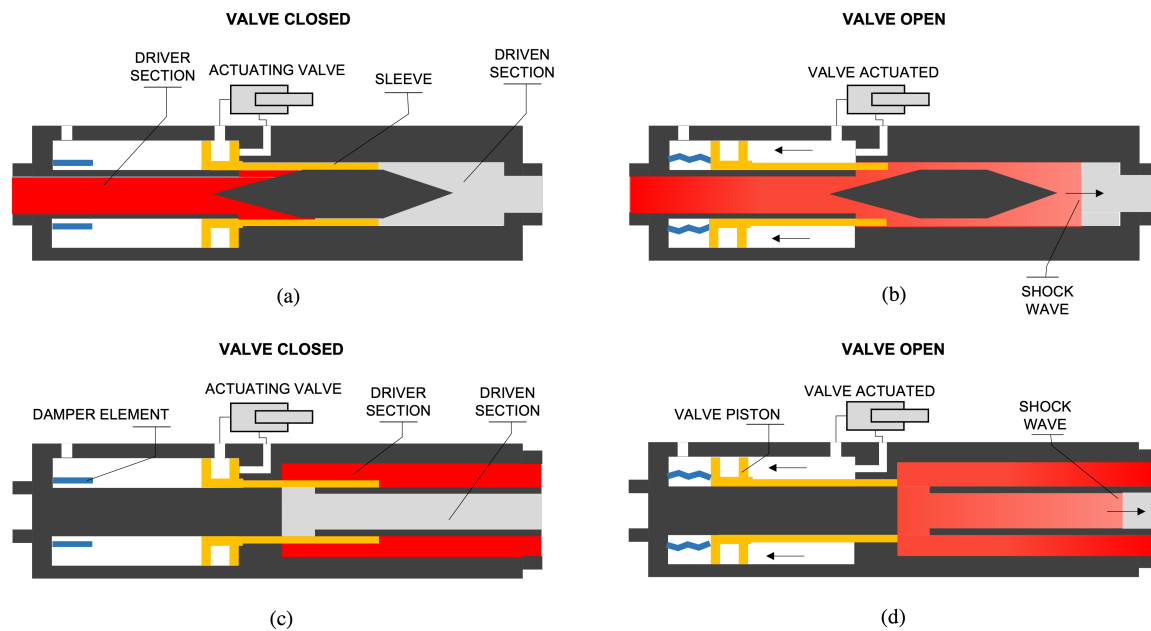


FIGURE 7. Sleeve-type fast-acting valve that is operated with actuating solenoid valves. The design proposed by Heufer et al.⁸⁴ is shown in (a) when the valve is closed and (b) when the valve is open (Adapted with permission from Springer Nature: Heufer et al.⁸⁴, copyright 2012). Unlike the inline driver-driven arrangement, Downey et al.⁸⁵ used the sleeve in a coaxial driver-driven configuration. Schematic diagrams of Downey et al.’s valve design in the (c) closed state and in the (d) open state (Adapted with permission from Springer Nature: Shock Waves, Downey et al.⁸⁵, copyright 2011).

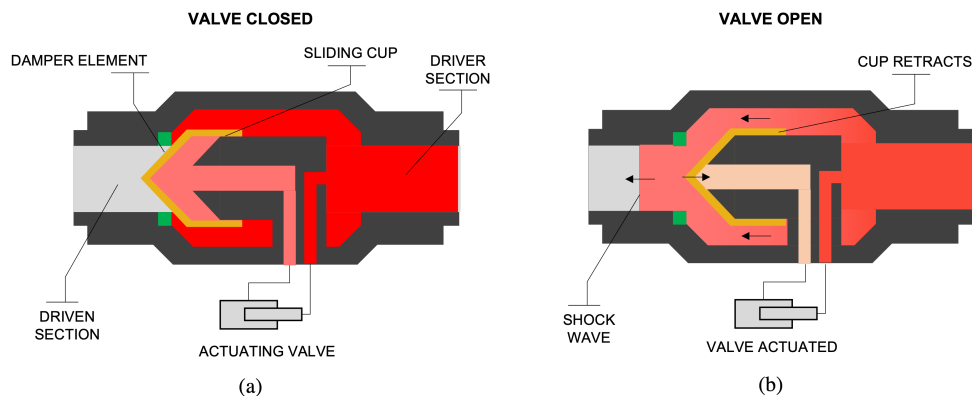


FIGURE 8. A commercially available high-speed valve design that can be mounted in line with the driver and driven section⁸⁹. (a) In the closed state, a sliding cup blocks the driver gas from entering the driven section. (b) When the volume of gas behind the sliding cup is exhausted, the cup retracts and shock wave is formed in the driven section.

designed for good reproducibility over thousands of shots. An improvement of the solenoid driver used in HRRST was suggested for a 12.7 mm bore shock tube⁹¹. Improved performance and cycle life were obtained using a new face o-ring sealing design, increasing the internal volume and providing inserts near the solenoid core. A more recent development of the solenoid actuated valve improved the longevity and simplified the maintenance and manufacture of the solenoid valve⁹². A pneumatic gas-driven diaphragmless shock tube with an operating mechanism similar to air gun technology was developed to produce weak shock waves⁹³. The table-top

arrangement had a dumbbell-shaped piston whose movement was controlled using a trigger and reservoir chamber. The actuator could be quickly reset, thus decreasing the experimental turnaround time. Fast-acting valves procured commercially have been used in diaphragmless shock tubes^{89,94–97} (see Fig 8). Amer and co-workers⁹⁷ compared the performance of fast-acting valves with conventional single and double diaphragm techniques. The shock-wave formation, repeatability, valve efficiency, and ease of operation were evaluated in their study. These valves were connected between the driver and driven section, replacing the diaphragm. The valves are available

for different internal diameters and can operate at high driver pressures of up to 100 bar. Recently, a commercial valve was used in a diaphragmless shock tube for chemical kinetics studies which showed that the repeatability of the reflected shock temperature was similar to that obtained using a double-diaphragm technique⁸⁹. A rapid opening shutter valve was developed and demonstrated in a 60 mm internal diameter diaphragmless shock tube⁹⁸. The innovative shutter valve was actuated electropneumatically and incorporated a feature that opened the valve from the center of the tube.

IV. DESIGN FEATURES OF FAST-ACTING VALVES

The main design features of a fast-acting valve include a closure element, an actuation mechanism, and the orientation of the driver and driven sections. These design features of various diaphragmless shock tube designs reported in the literature are consolidated in Table I. The design aspects of the valves are discussed in the following sections.

A. Closure element

Every valve design has an internal element that initially seals the pathway between the driver and the driven section. This element retracts on actuation and opens the pathway between the two sections of the shock tube. This movable obstruction is termed as a closure element⁹⁹. The actuator sets the closure element in position to separate the driver gas from the driven gas. When the actuator is toggled, the closure element quickly retracts to create an opening between the driver and the driven section. The closure element is either a piston (or seal plate), sleeve, cap, or membrane based on the various valve designs. The single and double piston arrangements have been widely used in diaphragmless shock tube designs. The piston is exposed to substantial forces, especially in the annular driver section, which requires stronger and heavy pistons. Kosing et al.²⁰ performed experiments with pistons made of solid brass (4.4 kg), solid PVC (0.71 kg) and hollow aluminium (0.38 kg). The aluminum piston was used only for low driver pressures. The piston designed by Alvarez et al.²¹ weighed 6.6 kgs and was used for driver pressures of up to 6 bar. Figure 4 shows different closure elements that can be utilized in the Oguchi-type valve. Although the piston with lip and plug provides good sealing, the seals get damaged frequently as they leave the sliding face during the operation. A sleeve valve member has lesser weight as compared to the pistons used in diaphragmless shock tubes. Heufer et al.⁸⁴ designed a sleeve made of aluminum which weighed about 3.124 kgs. Membranes are by far the lightest closure element for fast-acting valves. The elastic property of the membrane helps in achieving fast opening times. Rubber membranes are also self-sealing, unlike metallic pistons in which a groove has to be designed to accommodate a gasket or an o-ring. One of the main disadvantages of using a membrane is that the pressure difference across the membrane cannot be large, which restricts the maximum pressure used in the driver sec-

tion. Most of the rubber membrane valves have been tested for driver pressures less than 25 bar^{47,69,75,80}. Membranes also lose their elastic property with repeated use, limiting the valve's cycle life. Caps are used in compact valve designs, especially in scenarios where the driver section is in line with the driven section. The mass of caps is a few hundred grams, and caps have been used in commercial valves up to pressures of 100 bar. The advances in material science have brought about numerous lightweight metal alloys and composites with high strength and durability. These materials present a wide range of options for high-performance closure elements.

B. Actuation and control elements

The actuation and control elements are responsible for the movement of the closure element. The valve's actuator translates the input energy to the motion of the control element. The actuator should be powerful enough to overcome the force to move the closure element at a very high speed to match the time scales of a diaphragm rupture. Skousen⁹⁹ defined that the sizing of the actuator is dependent on the total force required to open the valve, given by,

$$F_{total} = F_{process} + F_{seat} + F_{friction} + F_{misc}. \quad (2)$$

where $F_{process}$ is the force to overcome unbalanced process pressures, F_{seat} is the force to provide correct seat load, $F_{friction}$ is the force to overcome frictional forces, and F_{misc} is the force to overcome certain design factors, such as the weight of the closure element, etc. The main types of systems that are used for valve actuation include hydraulic, pneumatic, electric, and electromagnetic¹⁰⁰. Table II highlights the advantages and disadvantages of these actuators. Hydraulic systems are suitable for heavy-duty purposes since compressing a fluid, such as oil, produces much more motion power than compressing a gas. Pneumatic systems cannot produce the power that hydraulic systems generate, but they are stronger than purely electric actuators. Pneumatic systems also tend to work faster than hydraulic and electric systems over the stroke of movement. Pure electric actuators (motor-driven) cannot match the power of hydraulic and pneumatic systems, though they are cleaner and can provide precise control over movement. Electromagnetic actuators include solenoid-based devices that are very reliable, quick, and commonly used. Overall, pneumatic and electromagnetic systems are preferred for diaphragmless shock tubes because they are fast, and their retraction motion can produce short opening times. The most common control element used for operating the fast-acting valves is solenoid valves (as seen in table I) that use electromagnetic actuation for quick action (about 1 – 5 milliseconds). The use of bellows has yielded good results for repeated operation as the motion of the closure element is consistent and reliable^{22,74,81,88}.

TABLE I. A consolidated table of various diaphragmless shock tube designs reported in literature.

Author/Year (Ref.)	Configuration	Closure element	Actuation elements	Control element	Driven tube dimensions ^a	Max. driver pressure ^b
Condit, 1954 ¹⁹	Type-I(a)	Piston	Poppet	Cam	ϕ 25.4 mm	\approx 41 bar
Condit, 1954 ¹⁹	Type-I(a)	Piston	Poppet	Cam	ϕ 431.8 mm	\approx 14 bar
Muirhead, 1964 ⁴¹	Type-I(a)	Piston	Auxiliary piston-cylinder	Cam	ϕ 50.8 mm	\approx 41 bar
Takano, 1984 ⁵⁸	Type-I(a)	Piston	Auxiliary piston-cylinder	Magnetic valve	ϕ 40 mm	9 bar
Kim, 1995 ⁸¹	Type-I(a)	Seal Plate	Opposed bellows	Pneumatic valves	\square 44.5 by 88.9 mm	3 bar
Rego, 2007 ^{35,60}	Type-I(a)	Piston	Auxiliary piston-cylinder	Solenoid valve	ϕ 100 mm	20 bar
Miyachi, 2012 ⁶⁵	Type-I(a)	Piston	Piston-cylinder/Magnets	Solenoid valve	ϕ 10 mm	8 bar
Tranter, 2013 ⁹⁰	Type-I(b)	Piston	Vespel Poppet	Solenoid	ϕ 6.35 mm	102 bar
Lynch, 2016 ⁹¹	Type-I(b)	Piston	Vespel Poppet	Solenoid	ϕ 12.7 mm	102 bar
Downey, 2011 ⁸⁵	Type-I(c)	Sleeve	Piston-cylinder	Trigger valve	ϕ 50 mm	200 bar
Yang, 1994 ⁷³	Type-I(d)	Membrane	Diaphragm burst	Vacuum pump	\square 60 by 150 mm	NA
Hariharan, 2010 ⁶⁹	Type-I(d)	Membrane	Diaphragm burst	Vacuum pump	ϕ 50 mm	25 bar
Teshima, 1993 ⁵⁹	Type-I(e)	Piston	Auxiliary piston-cylinder	Magnetic valves	ϕ 16 mm	16 bar
Kosing, 1999 ²⁰	Type-I(e)	Piston	Brake pad	Hydraulic cylinder	ϕ 56 mm	50 bar
Alvarez, 2015 ²¹	Type-I(e)	Piston	Auxiliary piston-cylinder	Solenoid valve	ϕ 165 mm	6 bar
Watanabe, 1995 ⁶³	Type-I(f)	Piston	Diaphragm burst	Release valve	Ann. 210 & 230 mm	5 bar
Hosseini, 2000 ⁸⁰	Type-I(g)	Membrane	Diaphragm burst	Vacuum pump	Ann. 80 & 100 mm	5.4 bar
Svete, 2020 ⁹⁴	Type-II(a)	Cap	Piston-cylinder	Solenoid valve	ϕ 40 mm	70 bar
Sembian, 2020 ⁹⁶	Type-II(a)	Cap	Piston-cylinder	Solenoid valve	ϕ 80 mm	50 bar
Amer, 2021 ⁹⁷	Type-II(a)	Cap	Piston-cylinder	Solenoid valve	ϕ 80 mm	20 bar
Distefano, 1970 ⁴³	Type-II(b)	Seal plate	Electromagnetic coils	Current in coil	ϕ 70 mm	NA ^c
Oguchi & Ikui, 1976 ^{44,45}	Type-II(b)	Piston	Piston-cylinder	Diaphragm burst	\square 100 by 180 mm	NA ^d
Taguchi, 2018 ⁷⁰	Type-II(b)	Piston	Piston-cylinder	Solenoid valve	\square 60 by 150 mm	3 bar
Heufer, 2012 ⁸⁴	Type-II(c)	Sleeve	Piston-cylinder	Solenoid valve	ϕ 45 mm	20 bar
Muirhead, 1964 ⁴¹	Type-II(d)	Piston	Auxiliary piston-cylinder	Cam	ϕ 50.8 mm	\approx 138 bar
Ikui, 1977 ²⁵	Type-II(d)	Piston	Auxiliary piston-cylinder	Electromagnet	\square 38 mm	1 bar
Maeno, 1980 ⁵⁴	Type-II(d)	Piston	Auxiliary piston-cylinder	Solenoid valve	ϕ 50 mm	20 bar
Onodera, 1992 ⁶¹	Type-II(d)	Piston	Piston-cylinder	Release valve	\square 60 by 150 mm	NA ^e
Shiozaki, 2005 ⁸³	Type-II(d)	Piston	Poppet	Solenoid	ϕ 2 mm	10 bar
Tranter, 2008 ⁷⁴	Type-II(d)	Piston	Bellow	Ball valve	ϕ 71 mm	\approx 2 bar
Hariharan, 2010 ⁶⁹	Type-II(d)	Piston	Piston-cylinder	Solenoid valve	ϕ 50 mm	25 bar
Fuller, 2019 ⁸⁸	Type-II(d)	Piston	Bellow	Solenoid	ϕ 102 mm	100 bar
Swietek, 2019 ⁹³	Type-II(d)	Piston	Piston-cylinder	Solenoid valve	ϕ 76.2 mm	5.5 bar
Zhang, 2020 ⁶²	Type-II(d)	Piston	Auxiliary piston-cylinder	Ball valve	ϕ 19.4 mm	NA
Yamauchi, 1987 ⁵⁵	Type-III(a)	Piston	Auxiliary piston-cylinder	Solenoid valve	ϕ 30 mm	20 bar
Hurst, 1993 ⁵⁶	Type-III(a)	Piston	Auxiliary piston-cylinder	Solenoid valve	\square 62 by 44 mm	\approx 21 bar
Matsui, 1994 ⁵⁷	Type-III(a)	Piston	Auxiliary piston-cylinder	Magnetic valve	ϕ 50 mm	NA
Udagawa, 2012 ⁸⁶	Type-III(a)	Piston	Auxiliary piston-cylinder	Solenoid valve	ϕ 2 mm / ϕ 3 mm	9 bar
Udagawa, 2015 ⁸⁷	Type-III(a)	Piston	Auxiliary piston-cylinder	Solenoid valve	ϕ 2 mm / ϕ 3 mm	9 bar
Garen, 1974 ⁴⁷	Type-III(b)	Membrane	Diaphragm burst	Vacuum pump	\square 18 mm / ϕ 36 mm	1 bar
Udagawa, 2007 ⁷⁵	Type-III(b)	Membrane	Diaphragm burst	Diaphragm puncture	ϕ 1 mm	2 bar
Bredin, 2007 ⁶⁸	Type-IV(a)	Piston	Auxiliary piston-cylinder	Ball valve	ϕ 135 mm	NA
Miyachi, 2012 ⁶⁵	Type-IV(a)	Piston	Piston-cylinder	Solenoid valve	ϕ 10 mm	8 bar
McGivern, 2019 ²²	Type-IV(b)	Piston	Bellow	Ball valve	ϕ 31.8 mm	8 bar
Abe, 2015 ⁶⁶	Type-IV(c)	Piston	Piston-cylinder	Ball valve	ϕ 10 mm	9 bar
Ojima, 2001 ⁶⁴	Type-IV(d)	Piston	Piston-cylinder	Diaphragm burst	\square 60 by 150 mm	9 bar
Ikui, 1977 ²⁵	Type-V(a)	Piston	Auxiliary piston-cylinder	Electromagnet	\square 38 mm	1 bar
Abe, 1997 ⁶⁷	Type-V(b)	Piston	Piston-cylinder	Solenoid valve	ϕ 82 mm	176 bar
Samimi, 2020 ⁹⁸	Type-V(b)	Shutter	Linear actuator	Pneumatic drive	ϕ 60 mm	20 bar

^a ϕ indicates circular cross-section, \square indicates square/rectangular cross-section, and Ann. indicates annulus between two diameters.

^b The max. driver pressure listed is not necessarily the maximum operating pressure of the driver but the max. pressure listed in the cited source.

^c Used in combustion drivers to produce M_S in the range of 8-14.

^d M_S ranging from 1.2 to 5.0 in air

^e Although the value of the driver pressure is not specified, the ratio P_{41} used in the experiments was 2.5

TABLE II. Comparison of different systems used for valve actuation.

	Hydraulic	Pneumatic	Electric	Electromagnetic
Advantages	Powerful Safe Self-contained	Fast over long strokes Economical Simple design	Quick and fast response Precise control Clean operation and no leaks	Reliable and robust Miniature and remote operation Cost-effective
Disadvantages	Fast over short strokes High maintenance Risk of leaks	Limited power Short cycle life Gas requirement	Low power Complicated design Expensive	Electromagnetic interference Sensitive to voltage Limited force

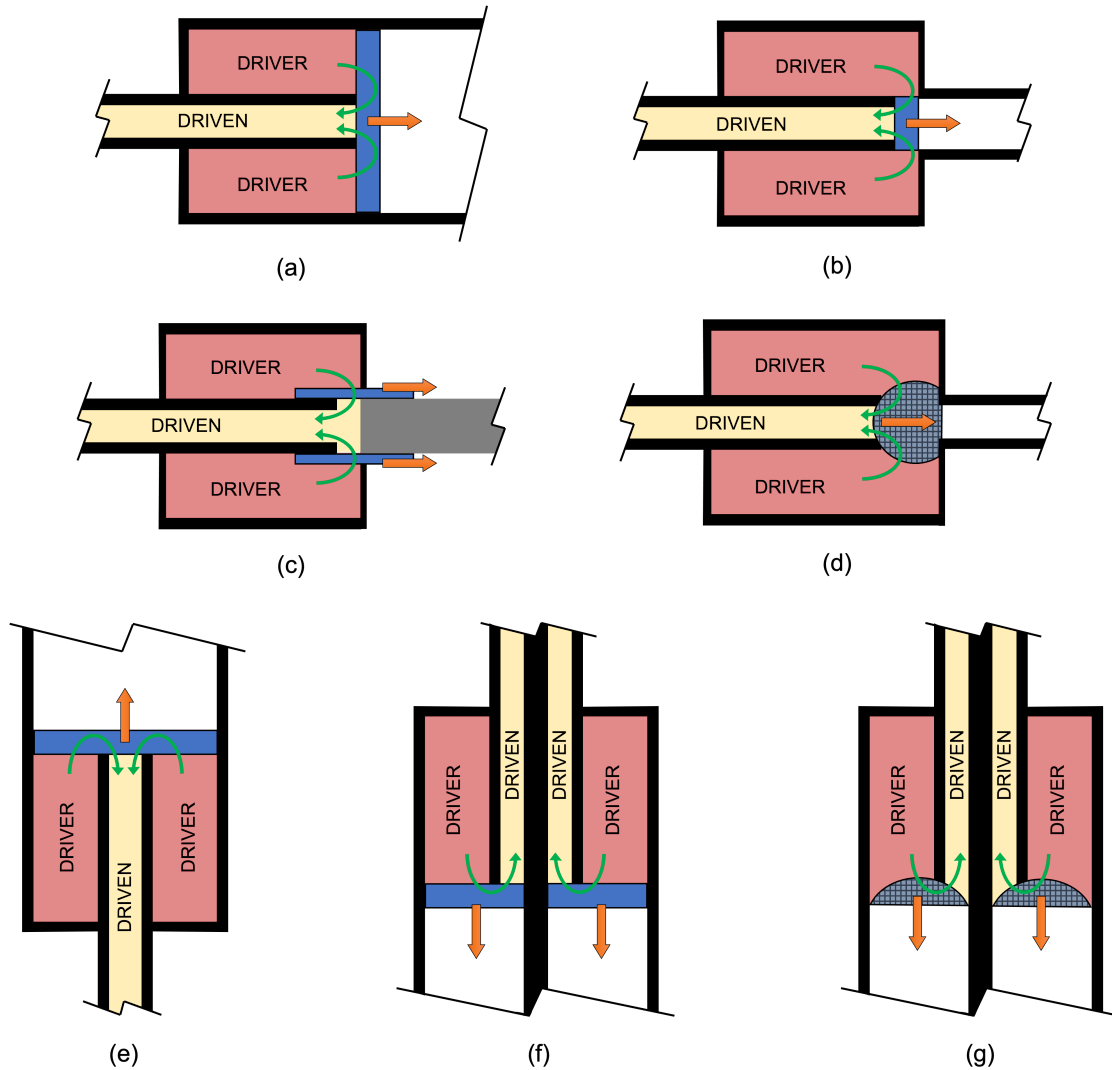


FIGURE 9. Schematic diagrams illustrating various Type-I configurations. The orange arrow indicates the movement of the element blocking the driver and driven section while the green arrows show the direction of flow after the movement of the element. (a) Piston-type configuration where piston is the size of driver section, (b) Piston-type configuration where the piston is the size of the driven section, (c) Sleeve-type configuration, (d) Membrane-type configuration, (e) Vertical configuration where piston moves against gravity, (f) Vertical configuration where piston moves in the direction of gravity, and (g) Vertical configuration where membrane retracts in the direction of gravity.

C. Driver-Driven configurations

The mounting configuration of the fast-acting valve and the driver’s placement relative to the driven section determines the

ease of gas flow from the high- to the low-pressure chamber. Although it would be ideal to have the two sections in line, the movement of the closure element may sometimes block the pathway. Based on the different designs reported in the literature, the driver-driven configurations can be arranged into five

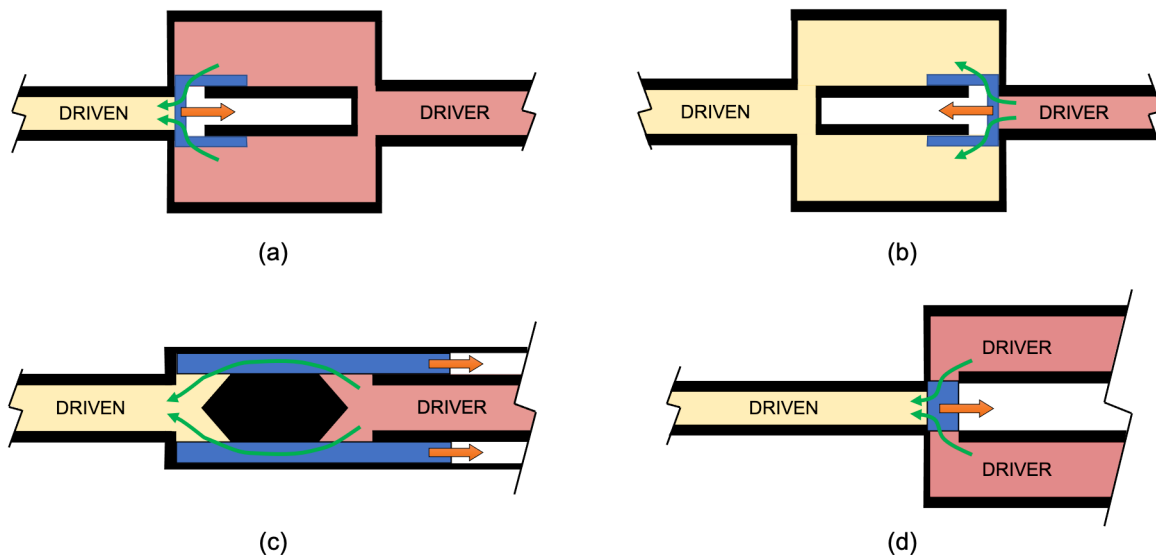


FIGURE 10. Schematic diagrams illustrating various Type-II configuration. The orange arrow indicates the movement of the element blocking the driver and driven section while the green arrows show the direction of flow after the movement of the element. (a) Cap-type configuration with variable cross-section driver section, (b) Cap-type configuration with variable cross-section driven section, (c) Sleeve-type configuration, and (d) Piston-type configuration.

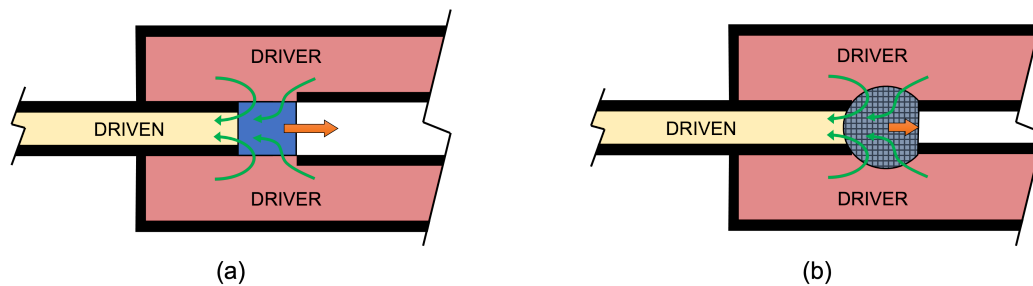


FIGURE 11. Schematic diagrams illustrating various Type-III configuration. The orange arrow indicates the movement of the element blocking the driver and driven section while the green arrows show the direction of flow after the movement of the element. (a) Piston-type configuration and (b) Membrane-type configuration.

categories.

1. Type-I driver-driven configurations

In this configuration, the driver gas is forced to take a 180° turn at the valve location. The flow redirection could lead to losses that eventually affect the strength of the shock wave generated in the driven section. The design proposed by Downey et al.⁸⁵ and Mejia-Alvarez et al.²¹ incorporated a curvature to streamline the flow to minimize the losses. Figure 9 shows schematic diagrams of variants under the Type-I configuration. In Type-I(a) configuration (see figure 9a), a large piston with diameter same as the inner diameter of the driver section seals the gases in the respective sections^{19,35,41,58,65,81}. The large piston size implies a larger force is required to move the piston to compensate for the mass. Takano et al.⁵⁸ suggested using a lightweight hollow piston made of aluminum for faster retraction speeds. Also, additional seals must be

used on the sliding face of the piston to prevent driver gas leaks. An important advantage of type-Ia is that the piston experiences a large force due to the driver gas in the direction of piston retraction. The piston size is smaller and comparable to the diameter of the driven section in Type-I(b) configuration (see Figure 9b). Face seals are sufficient to seal the driven section, and the low mass of the piston can help obtain faster retraction speeds. This configuration has been demonstrated in miniature shock tubes for driver pressures of up to 102 bar^{90,91}. The closure element in Type-I(c), as shown in Figure 9c, is a sliding sleeve on which the opposing forces for the sleeve movement are minimum due to the smaller exposed area. Downey et al.⁸⁵ employed this configuration to operate at high operating pressures of about 200 bar. Figure 9d shows a configuration with a rubber membrane. Yang et al.⁷³, and Hariharan et al.⁶⁹ used this configuration and obtained short opening times due to the quick retraction of the membrane. The cycle life and the limited pressure range of operation were some drawbacks of using the rubber membrane.

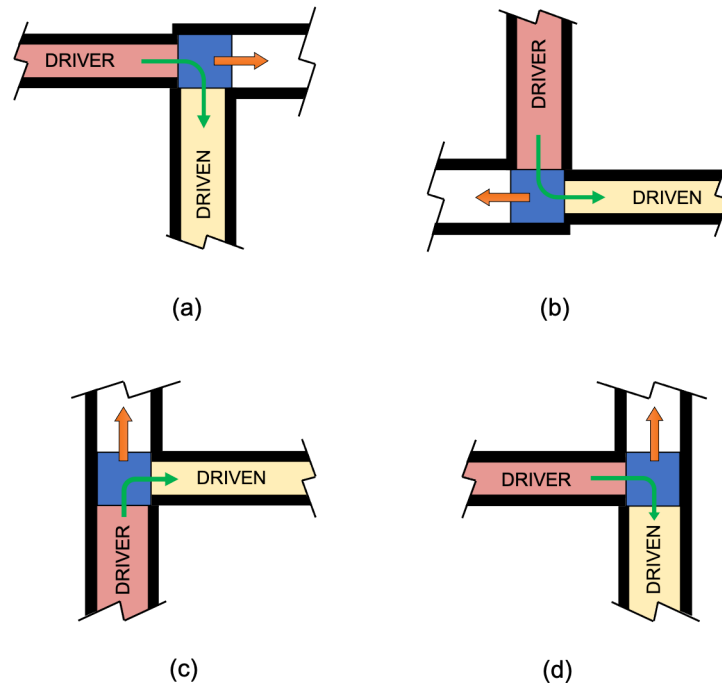


FIGURE 12. Schematic diagrams illustrating various Type-IV configuration. The orange arrow indicates the movement of the element blocking the driver and driven section while the green arrow shows the direction of flow after the movement of the element. Horizontal piston movement with (a) vertical driven section and (b) horizontal driven section. Vertical piston movement with (c) horizontal driven section and (d) vertical driven section.

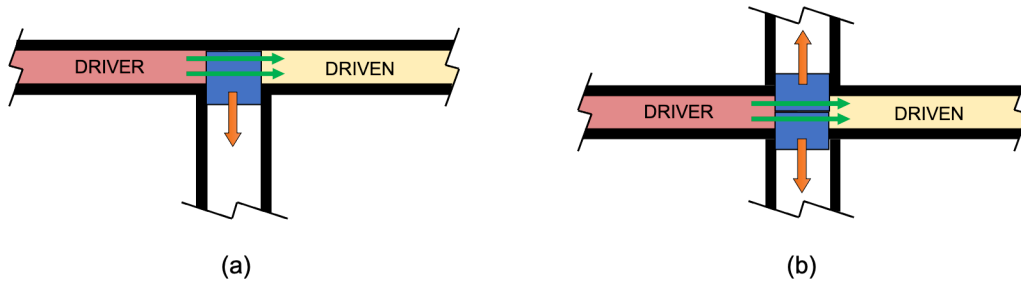


FIGURE 13. Schematic diagrams illustrating various Type-V configuration. The orange arrow indicates the movement of the element blocking the driver and driven section while the green arrows show the direction of flow after the movement of the element. (a) Movement of single element and (b) Movement of multiple elements.

Figures 9e and 9f show configurations of a piston-based valve for vertical shock tubes. In Type-I(e) configuration, the piston retraction is against gravity. The shock wave travels vertically downwards while the direction of piston movement and shock wave propagation is vice-versa in Type-I(f) configuration. The retraction force has to overcome the piston’s weight in Type-I(e) configuration^{20,21,59}. This configuration is ideal for vertical systems in studying shock wave interaction with liquids. Type-I(f) and I(g) configurations are used for the generation of annular shock waves using a piston⁶³ and membrane⁸⁰, respectively.

2. Type-II driver-driven configurations

The driver section is in line with the driven section in Type-II driver-driven configurations. Unlike the conventional diaphragm-type shock tube, the cross-section of the driver section is larger than the driven section. There is no major flow redirection compared to the type-I configurations. Therefore, there are fewer losses due to flow turning at the valve location. Generally, a streamlined path is provided in the valve to minimize resistance to flow. The variants of Type-II configuration are shown in Figure 10. Type-II(a) is a cap-type configuration, as shown in Figure 10a, which is adopted by many commercial valve manufacturers^{94,96}. This design allows the valve to be directly mounted in shock tubes that had

previously utilized a diaphragm by simply replacing the diaphragm section. The front face of the cap has a conical shape for streamlining the flow. The manufacturing tolerances and material selection in this design are critical to the operation of the valve. Type II(b) configuration is similar to Type II(a), but the driven section has a variable cross-section (see Figure 10b). The sleeve-type design (shown in Figure 10c) was reported by Heufer et al.⁸⁴. Compared to the cap-type and piston-type designs, one of the main disadvantages of this design is that the overall stroke length required to open the valve is much larger. Therefore, the valve is much longer, and a larger volume of gas has to be released from the actuating chamber during the operation. Figure 10d shows a piston-type configuration in which the piston retracts into an actuating chamber behind it. Numerous researchers have adopted this design because of its simplicity^{25,41,54,61,62,69,83}. The designs used by Tranter et al.⁷⁴ and Fuller et al.⁸⁸ are similar to those given in Figure 10d expect that the closure element does not retract into the actuating chamber but remains in the driver chamber. The schematics given in the figure mainly portray the driver-driven configurations. Figure 6 shows the actual depiction of Tranter et al.'s design⁷⁴.

3. Type-III driver-driven configurations

In Type-III configuration, a part of the driver section is annular to the driven section, and the rest of the driver section is in line with the driven section. Therefore, the flow of the driver gas is a combination of both scenarios seen in Type-I and Type-II configurations. Figure 11 shows the schematic diagrams of Type-III configurations. The piston-type (see Figure 11a) is more popularly used as compared to the membrane-type configuration (see figure 11b). The flow field in both cases is similar, except that the faster retraction of the membrane can lead to expansion waves in the region where the membrane is initially inflated. Supporting grids were used to limit the membrane's movement and eliminate these expansion waves due to the rapid movement of the membrane. A number of double-sliding piston design concepts use Type-II(a) configuration^{55-57,86,87} while the membrane-based design is reported by Garen et al.⁴⁷ and Udagawa et al.⁷⁵.

4. Type-IV driver-driven configurations

In this configuration, the driver gas undergoes a 90° flow turn as the driver and driven sections are perpendicular to each other. Figure 12 shows the schematic diagrams of Type-IV configurations. A long driver section is typically necessary to delay the rarefaction wave's interaction with the reflected shock wave. The 90° bend at the valve location may cause the rarefaction wave to interact with the contact surface too early and yield a decelerating shock. Hence, the alignment of the driver tube at a right angle is a disadvantage, as opposed to the straight-through flow path in configurations with in-line mounting. In Type-IV(a) and IV(b), the piston movement is horizontal, while the movement is vertical in Type-IV(c) and

IV(d). The driven section is vertical in type IV-(a) and IV-(d), while the driver section is vertical in type IV-(b) and IV-(c). The diaphragmless shock tubes proposed by Bredin et al.⁶⁸ and Miyachi et al.⁶⁵ utilized Type IV(a) configuration. McGivern et al.'s bellow-actuated shock tube²² has a vertical driver section attached to a 31.8 mm diameter driven section. Abe et al.⁶⁶ and Ojima et al.⁶⁴ employed Type IV-(c) and IV-(d) configurations, respectively.

5. Type-V driver-driven configurations

The best way to minimize resistance to the gas flow in the shock tube is by having the driver and the driven section of the same cross-section and in line with each other. Such a configuration ensures minimal losses in shock formation and propagation. In type V configuration (see Figure 13), the driver-driven chambers are in line, and the driver and driven sections' cross-sections are the same. Type V-(a) configuration, as shown in Figure 13a, has a single closure element that moves in the transverse direction. In type V-(a) configuration, the valve opening is asymmetrical about the shock tube axis. This design aspect of type-V(a) configuration makes it distinct from all the other configurations. The closure element is composed of multiple individual components in type V-(b) (see Figure 13b). Abe et al.⁶⁷ used two opposing pistons in their design. The design proposed by Samimi et al.⁹⁸ used a shutter configuration composed of either three or six blades. A substantial advantage of type V-(b) configuration is that the fast-acting valve opens from the center of the tube similar to the diaphragm-type shock tube operation. The transverse motion of the closure elements increases the loads on the seals due to the differential pressure. Ensuring proper sealing between multiple closure elements in type-V(b) is also challenging.

V. PERFORMANCE OF FAST-ACTING VALVES

The performance of diaphragmless shock tubes in terms of the opening time, shock formation distance, operating range, and shock wave conditions are discussed in the following sections.

A. Opening time of valve

The opening time of a fast-acting valve is an important parameter that determines the performance of the diaphragmless shock tube. It is the time taken by the closure element to move a distance that creates an opening with an area equal to the cross-sectional area of the driven section of the shock tube. Ideally, the opening time should be short so that a supersonic flow is initiated in the shock tube. The inability of commercial valves to produce such a condition through quick action makes them unsuitable for use in shock tubes. Therefore, customized fast-acting valves have to be designed for diaphragmless shock tubes. Determining the opening time of a fast-acting valve requires a dedicated optical measurement

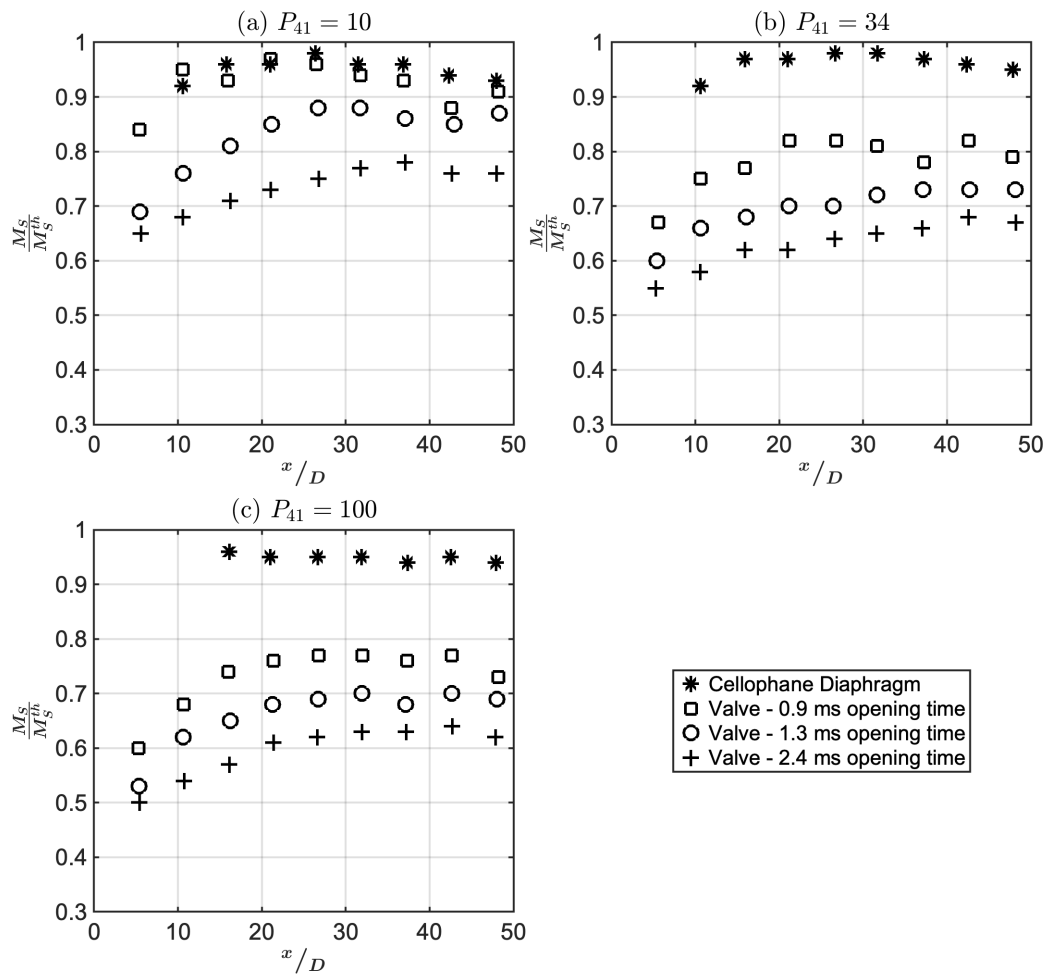


FIGURE 14. Variation of the normalized shock Mach number along the diaphragm-type and diaphragmless shock tube (M_S represents the experimental shock Mach number and M_S^{th} represents the theoretical shock Mach number obtained from 1D shock tube relations). (a) $P_{41} = 10$ (b) $P_{41} = 34$ (c) $P_{41} = 100$. (Reprinted with permission from The Japan Society of Mechanical Engineers: Bulletin of JSME, Ikui et al.²³, copyright 1979)

system. Since the closure element is enclosed in the driver or driven section, obtaining the opening time during the system's operation becomes challenging. Instead, in many cases, the movement of the closure element is monitored without mounting the driven section. Although this method does not give the valve's actual opening time, a rough idea can be obtained. In one of the early reports, the opening time was estimated using two laser beams and phototransistors as light detectors to track the retraction of the membrane⁴⁷. The opening time was estimated to be $460 \mu s$. Hariharan et al.⁶⁹ measured retraction speeds of about 8 m/s using high-speed photography for their membrane-based fast-acting valve. For a miniature 1 mm and 3 mm shock tube, the opening time of the rubber membrane valve was $46.6 \mu s$ and $117.2 \mu s$, respectively⁷⁷.

Piston-based diaphragmless valve concepts have slower speeds compared to rubber-membrane systems. Ikui et al.²⁵ performed a detailed investigation of the opening time as a

function of pressures used in different chambers. They reported opening times of less than ten milliseconds for a 38 mm square shock tube. Ikui and co-workers²³ also compared the variation of the shock Mach number along a diaphragm-type and diaphragmless shock tube at different P_{41} and valve opening times (see Figure 14). It is clear from the plots that the longer the opening time, the slower the shock propagation velocity. Also, at higher values of P_{41} , the deviation of the valve performance compared to the diaphragm-mode of operation is significant. Short opening times (< 2 milliseconds) are relatively simple to achieve in smaller diameter tubes ($< 10 \text{ mm}$) as the moving parts are lighter. The solenoid-based HRRST facility⁹⁰ has opening times of less than 1 millisecond for a 6.35 mm shock tube. The direction of movement of the closure element also has a vital role in the valve's opening time. Axial opening of the valve is preferred to gate-type opening because for the same distance traveled by the clo-

sure element, the flow area is more in the case of axial opening than transverse opening (gate-type opening). An example is the sleeve-based systems where the closure element has to travel a longer distance to completely open the valve (Sleeve moves about 100 mm stroke in the design reported by Heufer et al.⁸⁴). Abe et al.⁶⁷ reported an opening time of 1.79 milliseconds for a diaphragmless shock tube system that used an opposing piston. The short opening time results from the piston traversing only half the diameter of the shock tube and the high pressures to control the valve (greater than 150 bar).

B. Shock formation distance

Since measuring the opening time of the valve is challenging, an alternative method to evaluate the valve's performance is by measuring the shock formation distance. The shock formation distance is directly dependent on the opening time of the diaphragm in a conventional diaphragm-type shock tube^{26,31,101}. Although fast-acting valves do not open from the center of the tube (unlike the diaphragm rupture), a linear dependence between the opening time of the valve and the shock formation distance can be expected in a diaphragmless shock tube as well. This assumption holds good because the piston analogy for shock wave formation holds good for diaphragmless shock tubes. Ikui et al.²³ showed that the dependence of opening time and shock formation distance for diaphragm-type and diaphragmless shock tubes is linear (see Figure 15). The term M_{Smax} refers to the maximum shock Mach number obtained during the measurements. The shock formation distance (x_f) also depends on several other parameters indicated by the empirical and functional relationships reported in various studies.

$$x_f = t_{op} \cdot a_1 \cdot f(P_{41})^{102} \quad (3)$$

$$x_f = K_1 \cdot s \cdot t_{op}^{103} \quad (4)$$

where t_{op} is the opening time, a_1 is the speed of sound of the gas in the driven section, s is the shock speed, P_{41} is the ratio of initial pressure in driver and driven sections, and K_1 is a constant of proportionality. Verifying a fully developed shock wave is relatively simple compared to measuring the valve's opening time. It is generally done by mounting several pressure transducers along the driven section of the shock tube. The amplitude of the pressure trace and the calculation of the shock speed by the time-of-flight method can confirm the shock formation in the shock tube. The non-dimensional shock formation length is represented by the ratio of the shock formation length and the hydraulic diameter of the shock tube. The hydraulic diameter (d_h) of a shock tube is defined as,

$$d_h = \frac{4A}{PR} \quad (5)$$

where A is the area and PR is the perimeter of the cross-section. Typically, the shock formation distance in a diaphragm-type shock tube varies between 15-20 hydraulic

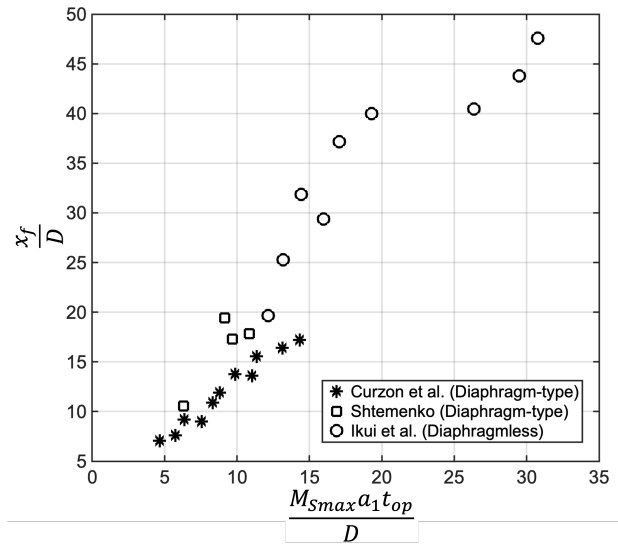


FIGURE 15. Dependence of shock formation distance (x_f) on the opening time (t_{op}) for diaphragm-type and diaphragmless shock tubes. (Reprinted with permission from The Japan Society of Mechanical Engineers: Bulletin of JSME, Ikui et al.²³, copyright 1979)

diameters¹⁰⁴. Longer shock formation distances are expected in diaphragmless shock tubes because of the slower opening times. Onodera reported a non-dimensional shock formation length of 65 for a composite piston-based diaphragmless shock tube⁶¹. The annular driver arrangement for a diaphragmless shock tube described by Alvarez and co-workers had a consistent shock formation at 41 diameters from the driver in the 165 mm diameter driven tube²¹. The diaphragmless shock tube based on a hydraulic brake pad mechanism had a non-dimensional shock formation length between 20 and 40²⁰ for different piston materials. A comparative study between a piston-based and membrane-based diaphragmless shock tube showed that the latter had a shorter shock formation distance⁶⁹.

Lynch et al.⁹¹ compared the shock pressure profiles obtained in a miniature shock tube using diaphragms and a fast-acting valve (shown in Figure 16(a)). The pressure profile obtained in non-reactive conditions using the diaphragmless driver (shown in blue in Figure 16(a)) is similar to the one obtained in the reactive conditions (shown in red in Figure 16(a)). However, a small hump is noticed after about 350 μ s compared to the shock profile obtained in the diaphragm-mode of operation (shown in magenta in Figure 16(a)). The valve opening characteristics are a possible reason for this observation. Non-ideal effects are more pronounced in the 6.35 mm diaphragmless shock tube that has a shorter driven section length (shock profile shown in green in Figure 16(a)). An essential aspect concerning the shock profile and duration is the intended application of the shock tube. If the primary information is extracted before distortions appear in the pressure profile, then the shape of the rest of the signal is of little consequence. Amer et al.⁹⁷ showed an improved shock profile with increased driven tube length. The difference in the shock pro-

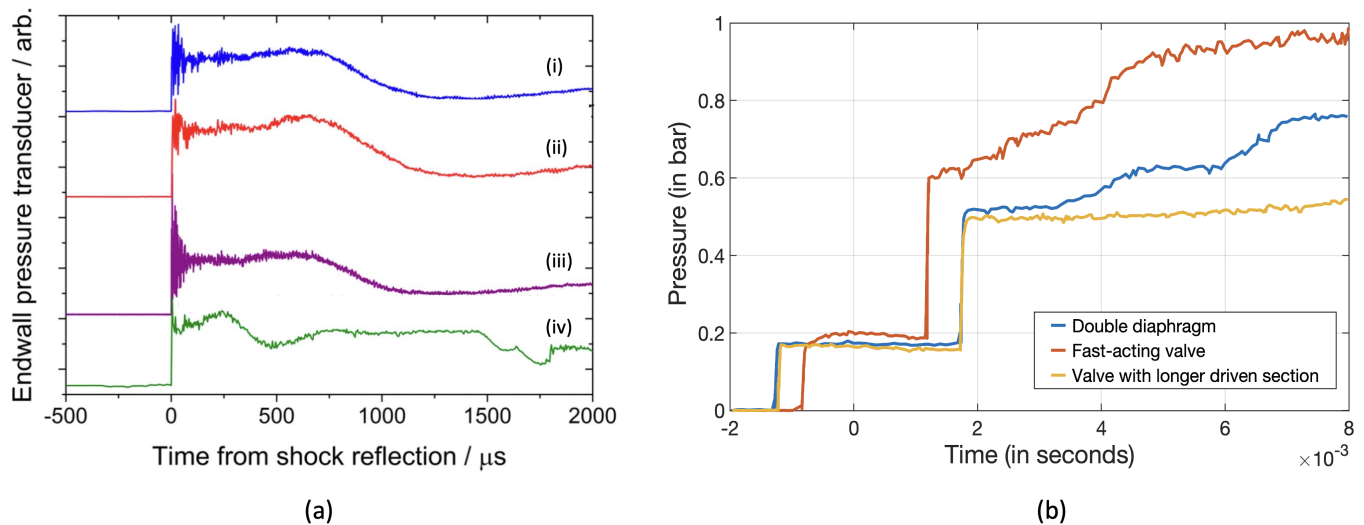


FIGURE 16. Comparison of shock profiles obtained using the diaphragmless and diaphragm-type shock tubes. (a) Experimental plots reported by Lynch et al.⁹¹. (i) 12.7 mm bore, modified solenoid driver⁹¹, 100% Ar (ii) 12.7 mm bore, modified solenoid driver⁹¹, 0.003 C₂H₃F₃/Ar (iii) 12.7 mm bore, diaphragm driver, 100 % Ar (iv) 6.35 mm bore, solenoid driver⁹⁰, 100% Ar, driven tube length shorter than that in the 12.7 mm shock tube. (Reprinted with permission from AIP Publishing: Review of Scientific Instruments, Lynch P. T.⁹¹, copyright 2016) (b) Experimental plots reported by Amer et al.⁹⁷. (Adapted with permission from Amer et al.⁹⁷)

files between the double-diaphragm and diaphragmless-mode operations in a 5 m long shock tube (driver length of 2 m and driven length of 3 m) is quite prominent. When the overall length of the shock tube is changed to 10 m (driver length of 3 m and driven length of 7 m), the shock profile resembles the one obtained in the diaphragm-mode of operation. The reflected shock pressure is relatively flat compared to that obtained in the double-diaphragm experiments.

C. Operating range, repetition rate and reliability

The operating range of diaphragmless shock tubes depends on the design features (driver-driven configuration, closure, actuation, and control elements) used in the fast-acting valve. Table I shows the maximum driver pressure used in the various diaphragmless shock tubes. It is essential to mention here that the value of maximum driver pressure listed in the table is simply the highest value of pressure used for the experiments. This value does not necessarily indicate the upper operating limit of the valve. Table I shows that diaphragmless shock tubes can operate at pressures as low as 1 bar to pressures of up to 200 bar. A helpful way to estimate the efficiency of the diaphragmless shock tubes is by determining the shock Mach number as a function of the initial conditions in the shock tube. It is generally seen that the efficiency of diaphragmless drivers is lower than diaphragm-type shock tubes²². Figure 17 compares the efficiency for different diaphragmless shock tubes. The experimental data are plotted against the one-dimensional inviscid relation shown in equation 1 (represented as a solid line in the figure). Experimental data from only a few reports have been used in the plot as

the working gas differs for different studies. Figure 17 shows that the performance of the diaphragmless shock tubes significantly deviates from the predictions beyond $P_{41} = 50$. Therefore, the performance of diaphragmless shock tubes at higher initial pressures needs to be improved.

The turnaround time between experiments is significantly reduced by using diaphragmless drivers. Incorporating a mechanism to bring the closure element back to its original position improves the turnaround time further. Using a secondary diaphragm to run a diaphragmless shock tube is a significant disadvantage in terms of the repetition rate^{44,45,75}. Amer and co-workers compared the turnaround times in shock tubes operated in single-diaphragm mode, double-diaphragm mode, and diaphragmless mode⁹⁷. They found that the operating time for their diaphragmless shock tube was about 6 min compared to about 32 min and 48 min for the single-diaphragm and double-diaphragm modes, respectively. Miniature diaphragmless shock tubes having a high-repetition-rate of 4-5 Hz have also been demonstrated^{83,90}. Figure 18 shows the repeatability obtained in a high-repetition-rate diaphragmless shock tube operated at 0.25 Hz. The cost and lifetime of the fast-acting valves are a couple of key points to consider while designing diaphragmless shock tubes. Since most fast-acting valves are customized designs, developed in laboratories and used solely for research purposes, their cost is not reported in the literature. The cost of commercial valves can be about a few thousand US dollars depending on the diameter of the valve. The high-repetition rate solenoid actuated driver valve has been tested for several thousand experiments⁹². The commercial fast-acting valve manufacturer claims the valve's lifetime to be at least 5 million shots. The scalability of the diaphragmless shock tube to

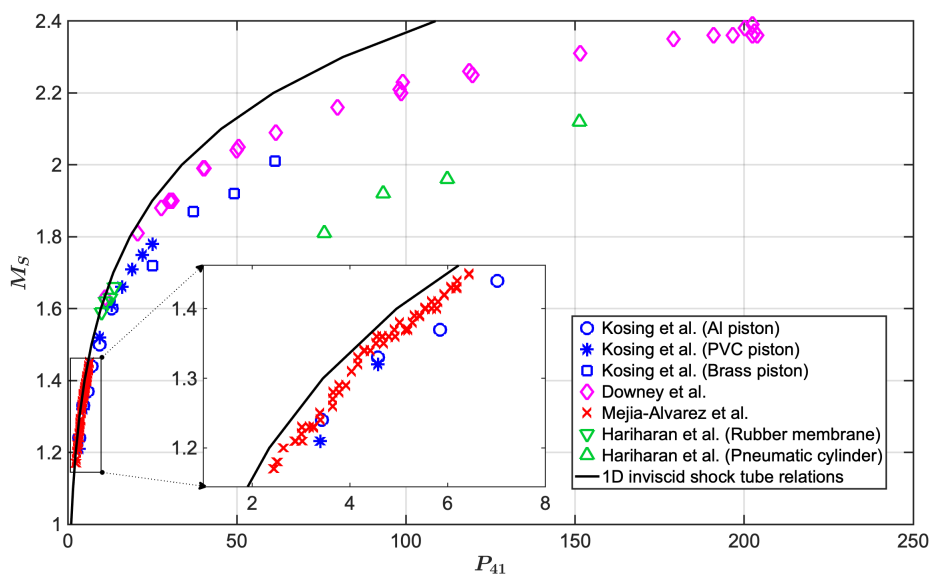


FIGURE 17. Driver efficiency for diaphragmless designs reported in literature for air as working gas. (Adapted with permissions from Springer Nature: Shock Waves Mejia-Alvarez et al.²¹ copyright 2015, from Springer Nature: Shock Waves Kosing et al.²⁰ copyright 1999, from Springer Nature: Shock Waves Downey et al.⁸⁵ copyright 2011, and from Springer Nature: Shock Waves Hariharan et al.⁶⁹ copyright 2010)

large diameters is essential in some applications. Commercial valves are currently available up to a maximum diameter of 80 mm.

D. Performance in reflected shock mode

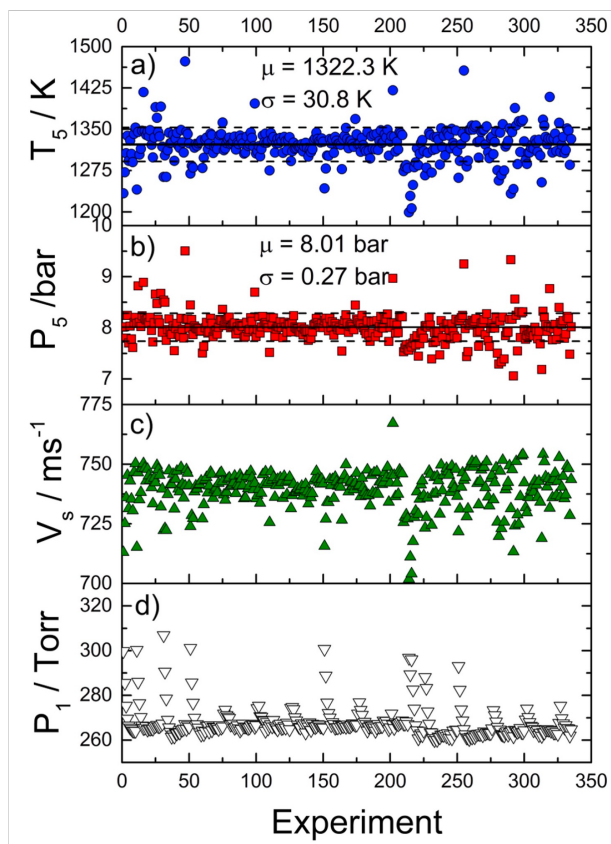
While shock tubes have several different applications, one of the primary uses is the study of chemical kinetics by the combustion community, which is often done in the reflected shock mode (utilizing the T_5 and P_5 conditions). In such experiments, key performance characteristics are the attenuation rate of the incident shock wave, the temporal dependence of the reflected shock pressure (dP_5/dt), and the duration of test-time. The attenuation of the incident shockwave is particularly important in determining the reflected shock temperature that is vital for chemical kinetics studies¹⁰⁵. In general, keeping the incident shock attenuation rate as low as possible is desirable to avoid a large axial temperature gradient. Similarly, dP_5/dt should be minimal to perform kinetic studies at conditions fairly close to the reflected shock (T_5 , P_5). Other performance aspects of diaphragmless shock tubes pertaining to chemical kinetics studies include the range of Mach numbers that can be obtained and the potential for tailoring to extend the reflected-shock test times. The range of Mach numbers obtained in the shock tube is directly related to the operating pressure range, as discussed in the previous section. A recent study investigated these reflected-shock characteristics by employing a newly developed diaphragmless shock tube to study combustion chemistry⁸⁹. The average dP_5/dt in the reflected shock region was about 2.5%/ms. The velocity er-

ror was about $\pm 0.224\%$, and the attenuation rate was about 0.41%/m. These values are comparable to those obtained using diaphragm-type shock tubes¹⁰⁶. In this work, the driver gas was tailored using nitrogen gas (18% by volume), as described in detail by Campbell et al.¹⁰⁷, to obtain longer test times for some of the fuel mixtures.

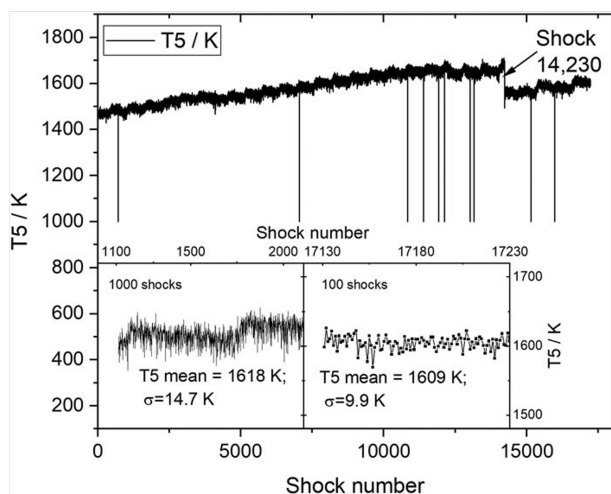
E. Improving valve performance

While diaphragmless shock tubes present several advantages over conventional shock tubes, there is still significant scope for performance improvement. The limitations discussed below are specific to certain design concepts. A valve design that addresses all such limitations without compromising performance and efficiency would be the most desirable.

- **Shortening opening times** - One of the main limitations of a diaphragmless shock tube, compared to a conventional shock tube, is that the time scales of the diaphragm rupture process cannot be matched. The opening time of fast-acting valves has to be improved to reduce the shock formation distance in the shock tube.
- **Avoid flow turning** - The configurations of the driver and the driven sections in a diaphragmless shock tube are not necessarily similar to the conventional shock tube (except for very few design concepts employing Type-V driver-driven configuration). The flow turning at the location of the fast-acting valve can lead to losses that will affect the strength of the shock wave produced



(a)



(b)

FIGURE 18. (a) Repeatability of signals obtained by Lynch et al.⁹¹ in a miniature diaphragmless shock tube operated at 0.25 Hz. Solid lines represent μ (mean value) while dashed lines represent $\pm\sigma$ (standard deviation) from μ . (Reprinted with permission from AIP Publishing: Review of Scientific Instruments, Lynch P. T.⁹¹, copyright 2016) (b) Reflected shock conditions from 17000 experiments as reported by Tranter and co-workers⁹². The insets show the mean and standard deviation of the reflected shock temperature for 1000 and 100 runs acquired at 1 Hz repetition rate. (Reprinted with permission from AIP Publishing: Review of Scientific Instruments, Tranter et al.⁹², copyright 2020)

and hence lowers the efficiency of the diaphragmless driver.

- Minimal flow obstruction** - The components of the fast-acting valve (closure, actuation, and control elements) obstruct the gas flow in the shock tube. Complex flow interactions lead to undesirable effects in the observation window of the diaphragmless shock tube.
- Higher operational pressures** - The operation range of diaphragmless shock tubes is limited because larger forces must be overcome at higher pressures to move the closure element. The actuators controlling the movement of the closure element become more bulky and expensive.
- Reduce shock wave attenuation** - The presence of obstacles at the driver-driven interface or the perpendicular orientation of driver-driven sections can result in the reflected expansion waves catching up with the moving shock front earlier than expected. This scenario can lead to faster attenuation of the shock wave.
- Avoid damage to seals** - The amount of wear and tear of a seal is dependent on the valve design. In most designs, the seals on the closure element are breached during the operation of the diaphragmless shock tube. Repeated operation of the diaphragmless shock tube can wear and tear these seals and other moving parts. Therefore, there is a need for constant maintenance of the parts while using diaphragmless shock tubes.
- Reduce noise during operation** - Pneumatically-driven fast-acting valves operate by the sudden exhaust of pressurized gases due to the actuating mechanism. This process can be extremely noisy, and sufficient measures must be taken to exhaust these gases.

VI. MATHEMATICAL MODEL FOR FAST-ACTING VALVES

Mathematical models for several diaphragmless driver configurations have been developed and verified previously. Rego et al.¹⁰⁸ developed a numerical model based on the motion equation to describe the piston sliding time against pressure ratio for a double-piston arrangement similar to Oguchi et al.'s design. Alvarez et al.²¹ developed a model to describe the variants of the Oguchi et al. designs. Portaro et al.¹⁰⁹ analyzed the performance characteristics of the sleeve-based diaphragmless shock tube driver proposed by Downey et al.⁸⁵ using computational fluid dynamics (CFD) simulations. A CFD study was also performed to evaluate the performance of Heufer et al.'s design⁸⁴ to give insights into the complex interaction of the sliding piston with the transient flow. Udagawa and co-workers developed a numerical model using the Runge–Kutta–Gill method to understand the motion of the rubber membrane-based valve⁷⁷. In another work, Udagawa et al. suggested a simplified model for a double-sliding piston diaphragmless driver. This section presents a generalized

model to describe fast-acting valves and applies to two popular driver configurations as test cases.

A typical fast-acting valve consists of a moving piston to block the driver and the driven section, a mechanism to pull the piston as quickly as possible, and a provision to engage the piston to barricade the sections between runs. In every fast-acting valve, the mechanism by which the piston is released is different. However, the pneumatically or electropneumatically operated piston is preferred in most cases. Following are the key requirements for a fast-acting valve used in a shock tube:

1. Short opening time (on the order of a few milliseconds)
2. Lightweight and high-strength piston
3. Simple and cost-effective auxiliary systems
4. Ability of components to withstand extreme environments like high operating pressure, temperature, and corrosive gases.

Mathematically, one can design a fast-acting valve based on a simple approach to derive the vital geometrical parameters per the operational requirements, considering the abovementioned criteria.

- Firstly, the minimum distance (x) moved by the piston has to be estimated (see Figure 20). The effective diameter (d) of the driven section determines the value of x . Consider a piston with a circular cross-section that seals the driven section passage. The retraction of the piston to open the valve thus traces a cylindrical pathway whose circumference offers the entry of fluid flow into the driven section. The circumference of the cylindrical pathway and the effective flow diameter required can be thus equated to extract the piston displacement as,

$$\begin{aligned} x\pi d &= \frac{\pi}{4}d^2, \\ x &= d/4. \end{aligned} \quad (6)$$

The distance moved by the piston is determined by matching the flow area open to the driven section using this approach.

- Secondly, the acceleration (a_p) required to move the piston of a certain mass (m_p) is expressed in terms of the distance moved (x) and the total time taken for this motion (this is essentially the valve opening time t_{op}). From Newtonian mechanics, the motion equation can be derived for a_p .
- Thirdly, a free-body diagram of the piston helps determine the forces acting on the different faces. The force contributions due to friction, self-weight, seat loading and other design-specific loads (as explained in section IV B) must be included. The force required to move the piston can be related to the acceleration as,

$$F \geq m_p a_p. \quad (7)$$

The piston's mass (m_p) can be reduced by having a high strength-to-weight ratio material or material with low density (ρ_p). There are various choices, including Teflon, polyurethanes, hard-plastics, aluminum, and carbon-fiber-reinforced thin-metal shells for the lightweight piston material.

- Finally, the mechanism to generate F is decided and engineered. Popular choices are electromagnetic force, spring assistance, and pneumatic drives. Here, a pneumatically operated piston is considered.

A. Case I: Annular driver configuration

The schematics of the model developed by Alvarez et al. are shown in Figure 19. A piston with a lip configuration is shown in the figure, although the model was extended to cases where a piston with a plug and sleeve was used as a closure element. Relevant geometric parameters are shown in Figure 19a. The position, speed and acceleration of the piston are easily related as,

$$a_p = \frac{du_p}{dt} = \frac{d^2x}{dt^2} \quad (8)$$

The free-body diagram of the pressures acting on the different faces of the piston before and after breaching the seals is shown in Figure 19b. Figures 19c and 19d show the conditions before and after the seals are breached. The pressure evolution in the control volumes CV_4 and CV_5 are determined by two ordinary differential equations as the gas is released through the back pressure valve. The acceleration of the closure element for the case of piston with a lip is obtained as,

$$\frac{du_p}{dt} = \frac{1}{m_p} [(A_{4a} + A_{4b}) \cdot P_4 + (A_t + A_w) \cdot P_3 - A_{5a} \cdot P_5 - w_p] \quad (9)$$

For a piston with a plug, the acceleration is,

$$\frac{du_p}{dt} = \frac{1}{m_p} [(A_{4a} + A_{4b} + A_w) \cdot P_4 + A_t \cdot P_3 - A_{5a} \cdot P_5 - w_p] \quad (10)$$

For a sleeve, the acceleration is,

$$\frac{du_p}{dt} = \frac{1}{m_p} [A_{4b} \cdot P_4 - A_{5a} \cdot P_5 - w_p] \quad (11)$$

where w_p is the weight of the piston. The equations for acceleration and pressure evolution are solved numerically to obtain the velocity and opening time of the diaphragmless valve.

B. Case II: Inline driver configuration

An internally held pneumatically operated annular fast-acting valve during the closing and opening is shown in Figure 20. The piston is initially at rest, so the initial velocity is $u = 0$. The piston should not throttle the flow to enter the driven section as it reduces t_t significantly. Hence, a part of the piston

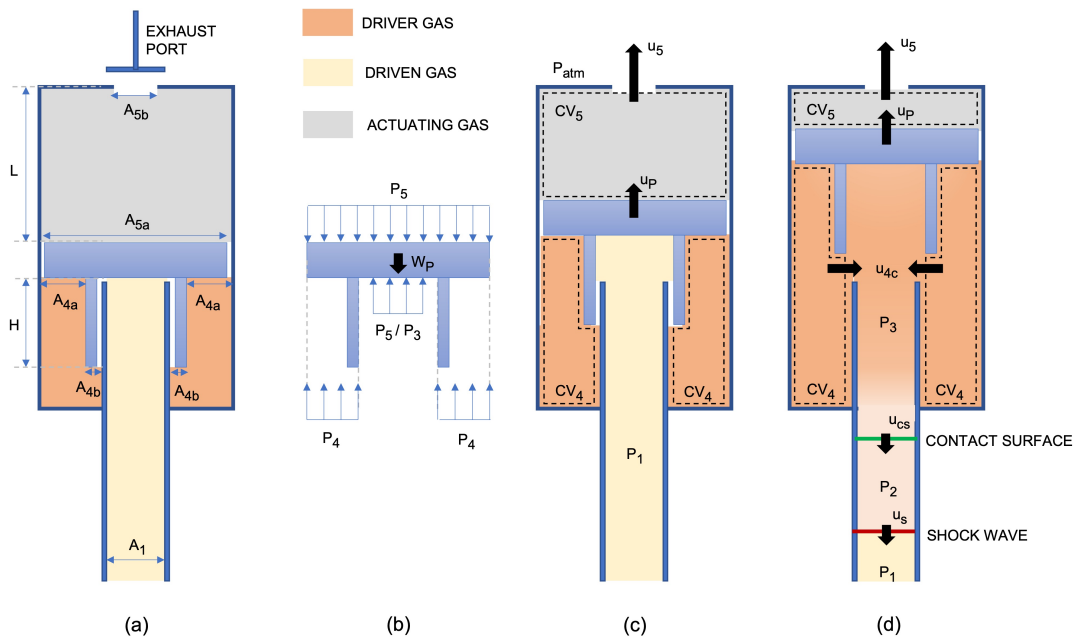


FIGURE 19. Schematic diagrams of the model developed by Mejia-Alvarez et al.²¹ (a) Relevant geometric parameters. (b) free body diagram of the piston; P_1 contributes before valve opening; P_3 replaces P_1 after valve opening. (c) Conditions before seals are breached. (d) Conditions after seals are breached. (Adapted by permission from Springer Nature: Shock Waves, Mejia-Alvarez et al.²¹, copyright 2015)

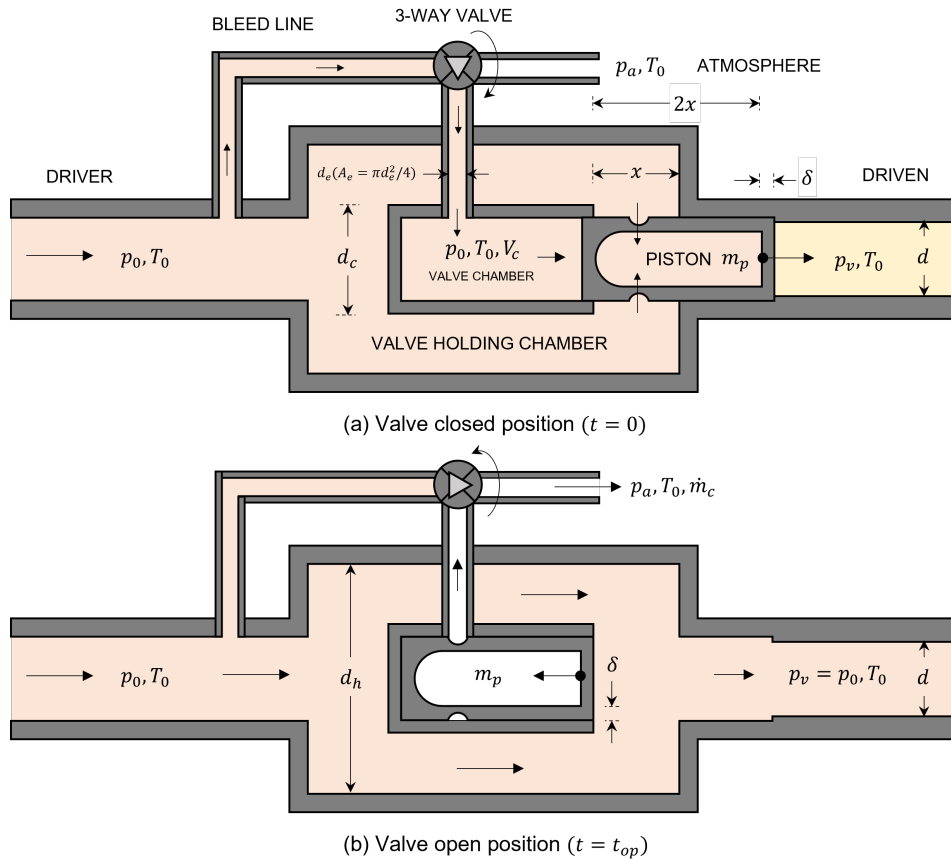


FIGURE 20. Schematics showing the vital geometrical and physical parameters involved in the (a) closing and (b) opening operation of a typical fast-acting valve (Type-IIa, however, the parameters mostly remain the same).

is extended so that it runs x times deep into the driven section instead of exactly closing in front of the driven section. In this manner, the tip of the piston, upon retracting from the driven section entrance, already possesses sufficient velocity and quickly allows the driver gas to enter the driven section. The desired a_p is then calculated as,

$$\begin{aligned} 2x &= ut_v + \frac{1}{2}a_p t_v^2, \\ a_p &= \frac{4x}{t_v^2}. \end{aligned} \quad (12)$$

For the present configuration, after considering the hemispherical dome-end and perforation, m_p is calculated as,

$$\begin{aligned} m_p &\lesssim \frac{\pi \rho_p}{4} \left[d^2(2x+2\delta) - \dots \right. \\ &\quad \left. \dots (d-2\delta)^2 \left(2x - \frac{d-2\delta}{2} \right) - \frac{(d-2\delta)^3}{3} \right]. \end{aligned} \quad (13)$$

The mass per unit density of the piston is calculated by subtracting the volume of the outer cylinder from the sum of the inner cylinder and the inner hemispherical dome-end. Additionally, the piston mass variation due to the peripheral perforation is considered negligible. Considering the calculated a_p and m_p in the previous steps, the net force is given by

$$F \gtrsim \frac{4xm_p}{t_v^2}. \quad (14)$$

The piston enclosed in the valve chamber retracts quickly upon exhausting the gas pressure in the chamber, as the surrounding driver gas and the suction pressure produce the necessary force to move the piston. The time scale of gas exhaustion should be smaller than the valve opening time scale. The valve's performance can be further improved by exhausting the gas into a pre-evacuated chamber (typically ≤ 0.1 Torr). Smaller the valve chamber volume (V), the quicker the exhaustion and, thus, the piston's movement. The total time (t_0) required to empty V is calculated from the mass conservation law or continuity equation in fluid dynamics as,

$$t_0 = \frac{2}{k(\gamma-1)} \int_{r^*}^r (r^2+1)^{(2-\gamma)/(\gamma-1)} dr + t_c, \quad (15)$$

where,

$$\begin{aligned} r^* &= \sqrt{\frac{\gamma-1}{2}}, \\ r &= \sqrt{\left(\frac{p_0}{p_a} \right)^{\frac{\gamma-1}{\gamma}} - 1}, \end{aligned}$$

$$k = \frac{-\gamma A_e}{V_c} \left(\frac{2\gamma RT_0}{\gamma-1} \right)^{\frac{1}{2}} \left(\frac{p_0}{p_a} \right)^{\frac{\gamma-1}{2\gamma}},$$

$$t_c = \frac{V_c}{A_e \sqrt{\gamma RT_0}} \left(\frac{2}{\gamma-1} \right) \left(\frac{\gamma+1}{2} \right)^{\frac{\gamma+1}{2(\gamma-1)}} \left[\left(\frac{p_0}{p_c} \right)^{\frac{\gamma-1}{2\gamma}} - 1 \right].$$

Here, A_e represents the exhaust piping cross-sectional area ($\pi d_e^2/4$), γ is the specific heat ratio, R (J/kg/K) is the specific gas constant, and p_c is the critical total pressure required to choke the flow in the exhaust duct. Value of V_c in the considered case is calculated as,

$$V_c = \frac{\pi}{4} d^2 (2x+2\delta). \quad (16)$$

For the current case, other geometrical parameters like the valve-holding chamber dimension are calculated based on d and d_c , where d_c is the outer diameter of the valve chamber. It has to be noted that d_c is larger than d . The effective diameter and the annular diameter of the valve-holding chamber can be equated to avoid local choking. Assuming $d_c \sim d$, d_h is given as,

$$\begin{aligned} \frac{\pi}{4} (d_h^2 - d_c^2) &= \frac{\pi}{4} d^2, \\ d_h^2 &= d^2 + d_c^2 \sim 2d^2, \\ d_h &\gtrsim \sqrt{2}d. \end{aligned} \quad (17)$$

The piston is held in the valve chamber as a concentric slider with a 0.05-0.1 mm tolerance. The sliding piston offers negligible frictional force and allows light gas leakage for the considered short-time operation. During the valve-closed operation, the gas fills the valve holding chamber and valve chamber with the same driver pressure (p_0). The body of the piston is perforated or made of small holes such that the driver gas fills it. Upon releasing the 3-way valve, a fast-acting pneumatic valve with an opening time of 3-30 ms (e.g., Festo® fast-switching valves-MH series), the valve chamber gas exhausts into the atmosphere rapidly. As mentioned earlier, the valve performance can be further improved by exhausting the gas into a pre-evacuated chamber. The net force acting on the piston ends is the same due to how they are shaped. The end that faces the valve chamber is hemispherical, thus the net force F_v is

$$F_v = (p_0 - p_a) \left[2\pi \left(\frac{d-2\delta}{2} \right)^2 \right]. \quad (18)$$

Similarly, the end that faces the driven section is flat, and thus the net force F_d is

$$F_d = (p_0 - p_v) \left[\frac{\pi}{4} (d-2\delta)^2 \right]. \quad (19)$$

For $p_0 > p_a$ and $p_v \sim 0$, the net resulting force acting on the sides of the piston is the same ($F_v = F_d$). Given that $F_v > F$, the piston moves back into the valve chamber upon the actuation of the 3-way valve resulting in the opening of the fast-acting valve. In summary, as long as the time scales of valve chamber depressurization and of opening the 3-way valve are less than the desired valve-opening time, the fast-acting valve operates fine.

Let us consider a simple case to understand the design and sizing of parameters for a typical fast-acting valve for an inline driver configuration type which is the most commonly

TABLE III. Input parameters for the fast-acting valve design.

Parameters	Values
Effective tube diameter (d)	25 mm
Working gas (γ, R)	air (1.4, 287 J/kg/K)
Driver pressure (p_0) & temperature (T_0)	2 bar, 300 K
Driven pressure (p_v) & temperature (T_v)	~ 0 bar, 300 K
Ambient pressure (p_a) & temperature (T_a)	1 bar, 300 K
Desired uniform piston wall-thickness (δ)	3 mm
Piston material density - Teflon [®] (ρ_p)	2200 kg/m ²
Desired valve opening time (t_v)	3 ms

TABLE IV. Output parameters for the fast-acting valve design.

Parameters	Values
Equivalent displacement (x)	6.35 mm
Piston acceleration required (a_p)	2822.22 m/s ²
Mass of the piston (m_p)	14.7 g
Force needed to move the piston (F)	41.46 N
Holding chamber diameter (d)	35.9 mm
Holding chamber volume (V_c)	9.48×10^{-6} m ³
Pressure and vacuum side force ($F_d = F_v$)	59.9 N

used arrangement in aero/gas-dynamic testing facilitates. Figure 20 shows the vital design parameters. The desired input parameters are given in Table III. From equations 6-7, and 12-19, the key design parameters are computed and tabulated in Table IV. The valve design will be effective if a suitable material for the casings and the piston is chosen. The number of fill holes in the piston rod can be as many as the surface of the piston-rod supports. A notable advantage is that the gas fills the piston-rod interior rapidly, making the piston lightweight, e.g., $m_p = 14.7$ g in the present case.

Overall, the mathematical model described will come in handy while developing customized fast-acting valves based on the desired application and is a useful guide to follow prior to the fabrication of the valve. An important point to note is that the opening times calculated by the above procedure provide a first-order approximation of how quickly the valve might open. Several additional factors that influence the valve opening time are difficult to estimate accurately. Some useful recommendations based on the mathematical model are to have a lightweight closure element, minimize the surfaces on the closure element that lead to unwanted forces opposing the net retraction force, reduce the friction due to seals and incorporate a small clearance distance so that the closure element accelerates before breaching the seal. Other recommendations to improve the valve's aerodynamics include streamlining the flow and driver-driven configurations to ensure minimal flow turning. Material selection is also important in valve design. For example, high-enthalpy aerodynamic testing facilities generally operate at temperatures above ambient. Commercial fast-acting valves have limitations while continuously operating above 400-500 K. Suitable thermal resistant materials can be employed in these cases, and the fast-acting valve design can be tailored appropriately to suit the

application needs.

VII. SHOCK WAVE APPLICATIONS USING DIAPHRAGMLESS SHOCK TUBES: CURRENT TRENDS

The advantages of diaphragmless shock tube drivers made them a desirable candidate to replace the diaphragm-type mode of operation. Additionally, they have opened a range of new applications which were not previously possible with conventional shock tubes. The new possibilities that have emerged due to the high reproducibility, fast repetition, cleaner flow characteristics, and precise control are described in the subsequent sections.

A. Reliable studies in shock wave chemistry and physics

Shock tubes can produce conditions that cover a wide temperature and pressure range and provide time scales suitable for studying various chemical reactions. Some shock tube investigations include temperature dependence of the reaction rate constants, emission/absorption spectra of various reaction intermediates, ignition delay times of pure substances and distillate fuels, and mechanisms of many elementary reactions. In these studies, the shot-to-shot fluctuation of the thermodynamic properties behind the reflected shock in a conventional diaphragm-type shock tube can affect the quality of the acquired kinetic data. Since several gas properties are monitored at a fixed condition, comparing data at the same condition becomes a problem if the experiments cannot be precisely replicated. Therefore, using diaphragmless shock tubes in chemical kinetics studies is advantageous, and the unique diaphragmless shock tube design concepts described in this review facilitate these investigations. Yamauchi et al.'s diaphragmless shock tube was used for emission spectra studies in reproducible shock heated conditions⁵⁵. This facility was also used to improve the kinetic data at higher temperatures up to 3197 K^{110,111}. Matsui and co-workers⁵⁷ used a combination of a diaphragmless piston-actuated shock tube, excimer laser photolysis, and Atomic Resonance Absorption Spectrometry (ARAS) to study individual elementary reactions. The bellow-based diaphragmless shock tube developed by Tranter and co-workers⁷⁴ demonstrated the ability of a diaphragmless shock tube to obtain kinetic data in the low-pressure limit. A comparison between the rate coefficients obtained using the diaphragmless and diaphragm-modes is shown in Figure 21. Janardhanraj et al.⁸⁹ also demonstrated using a diaphragmless shock tube to measure ignition delay times in methane and n-hexane oxidation. The level of control on the operating conditions allowed the post-shock pressure to be constrained to a much narrower range for a wide range of temperatures than a conventional diaphragm-type shock tube. The diaphragmless shock tube was also coupled to a TOF-MS (Time-of-flight Mass Spectrometer), which allowed signal averaging over multiple experiments¹¹². This application was, again, not possible with a conventional shock tube. The

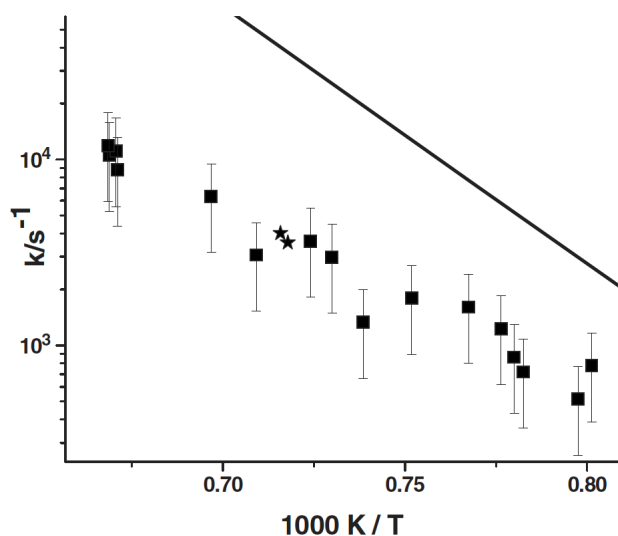


FIGURE 21. Rate coefficients for the dissociation of fluoroethane reported by Tranter et al.⁷⁴. Solid squares are data points obtained from diaphragm-mode of operation¹¹², solid stars represent data obtained from diaphragmless driver section and solid line represents k_{∞} ¹¹². (Reprinted with permission from AIP Publishing: Review of Scientific Instruments, Tranter et al.⁷⁴, copyright 2008)

work by Shaik et al.¹¹³ studied fluid dynamic effects in miniature tubes using synchrotron-based X-ray absorption, which is not possible with a conventional shock tube. Some other important studies that demonstrate the use of diaphragmless shock tubes in chemical kinetics include investigations of the decomposition of styrene¹¹⁴, reactions of propyl radicals¹¹⁵ and butyl radical isomers¹¹⁶.

The HRRST (high repetition rate shock tube) facilitated high temperature, high pressure, gas-phase experiments at facilities such as synchrotron light sources where space is limited, and many experiments need to be averaged to obtain adequate signal levels⁹⁰. The diaphragmless shock tube facility was designed to generate reaction conditions of $T > 600$ K, $P < 100$ bars at a cycle rate of up to 4 Hz. The benefits of shock tube/TOF-MS research were extended to include synchrotron-sourced PI-TOF-MS (Photo Ionization Time-of-flight Mass Spectrometer) as well¹¹⁷. The HRRST facility has also been widely used for other studies, which include chemical thermometry using 1,1,1-trifluoroethane dissociation⁹¹, ignition delay measurements¹¹⁸, kinetic modeling of ignition¹¹⁹, and pyrolysis studies using double imaging photoelectron/photoion coincidence spectroscopy¹²⁰. High-repetition shock waves produced by an automated diaphragmless shock tube have also facilitated molecular beam scattering experiments⁸³. Diaphragmless shock tubes have been successfully used in gas dynamic laser (GDL) experiments^{35,54,60,121} as, in addition to the high reproducibility of signals, they also limit the impurities inside the shock tube. The diaphragmless shock tube compresses and pre-heats a mixture instantaneously to elevated pressure and temperature in these experiments. The mixture

is delivered to a nozzle where the rapid cooling of the hot gas creates a population inversion and produces a laser medium. The precise control over the shock wave generation process in the diaphragmless shock tubes also allows for the synchronized operation of two shock tubes, as demonstrated by Maeno and Oguchi⁵⁴. In conventional shock tube operation, the water vapor from ambient air enters the shock tube during diaphragm replacement and freezes on the shock tube walls. The use of diaphragmless shock tubes can avoid water vapor contamination and is ideal for studies of low-temperature gases¹²².

B. Exploring shock waves in miniature scales

The interest in exploring shock wave phenomena in millimeter regimes springs from numerous interdisciplinary applications of shock waves in biology and medicine. Unlike large-scale shock tubes, the flow in miniature shock tubes is dominated by wall effects, and the attenuation of shock waves at these length scales has been investigated in recent years. Most of the studies utilize channels mounted at the end of a large diameter shock tube to study the propagation of shock waves in small-scales^{34,123,124}. It would be more pertinent to produce the shock waves in a miniature shock tube as it would not be practical to use a large-scale shock tube for miniature shock wave applications. As highlighted earlier (in section I), the smaller exposed area in miniature shock tubes poses a problem for the choice of diaphragm material and thickness. Therefore, a fast-acting valve is the best method to produce shock waves in miniature shock tubes. The studies performed in the 6.35 mm shock tube^{90,117}, 12.7 mm shock tube^{91,118,119,125}, and 8 mm shock tube¹²⁰ are great examples of the use of fast-acting valves in miniature shock tubes. Udagawa and co-workers⁷⁵ used a rubber membrane-based diaphragmless shock tube with an internal diameter of 1 mm to study the formation and propagation of shock waves in small-scales tubes. They observed weak dispersed shock waves using laser differential interferometry to detect the shock wave densities. They extended their work to observe shock waves and contact surfaces in a 3 mm internal diameter small-scale shock tube over a range of pressure conditions using the interferometric signal measurement with the collimated and polarized laser beams⁷⁸. The precise control of the operating pressure conditions in the diaphragmless shock tube allowed measurements over a range of pressures. This study confirmed that the shock waves do not propagate at constant velocity in this mini-shock tube. The attenuation of the shock waves in a 1 mm shock tube was also studied by a completely transparent driven section, generating the shock wave using a diaphragmless driver⁷⁶. The propagation characteristics of the shock wave in small diameter shock tubes were studied using a double-piston diaphragmless driver based on Oguchi's design⁸⁶.

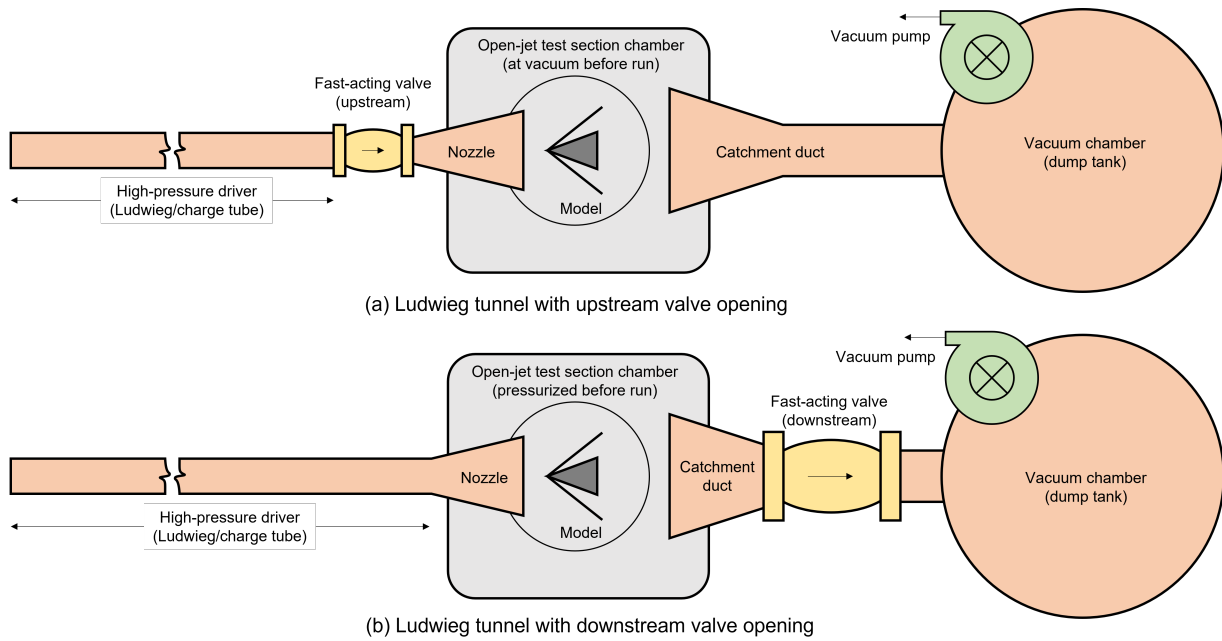


FIGURE 22. Typical schematics of Ludwig tunnel to realize hypersonic flow in the test-section in two different configurations with the fast-acting valve placed (a) upstream and (b) downstream. Some of the vital components that constitute to the construction of the hypersonic Ludwig tunnel are also shown in the schematics.

C. Automating aerodynamic ground test facilities

Many ground testing impulse facilities incorporate a diaphragm burst to initiate the flow for aerodynamic studies. Shock tunnels, free-piston shock tunnels, and Ludwig tunnels have started replacing the diaphragm with fast-acting valves to automate the facility and avoid damage to test models by the impact of diaphragm fragments. A Ludwig tube/tunnel is a short-duration aerodynamic test facility that produces high-speed flows between 100-1000 m/s for a 10-1000 milliseconds test duration. The total flow temperature can be maintained between 105 K and 1800 K. An automated Ludwig tunnel (see Figure 22) consists of five essential components: 1. Driver or Ludwig tube where the test gas is stored at high pressure, 2. Fast-acting valve whose response time is on the order of a few milliseconds (3-10 ms), 3. A converging-diverging (CD) nozzle accelerates the test gas to hypersonic velocity, 4. A test-section chamber to house the model under investigation, and 5. A vacuum or dump tank is kept at low pressure (on the order of millibars). Sometimes the test section and the vacuum tank are constructed as a single piece. The high pressure in the driver tube and the low pressure in the vacuum chamber facilitate an under-expanded hypersonic jet that emerges from the CD nozzle for a short duration once the fast-acting valve opens (see Figure 23). The expansion wave propagates in the driver tube to establish a constant total pressure and temperature (p_0 , T_0) in the tube. The reflected expansion waves reach the fast-acting valve to complete the test duration given by,

$$t_r = \frac{2L}{a}, \quad (20)$$

where t_r is the run-time, L is the driver tube length, and a is the sound velocity at that temperature.

A fast-acting valve at high-enthalpy conditions is preferred in modern hypersonic testing facilities like the Ludwig or shock tunnels. However, the high stagnation temperature encountered at the end of the tube poses limitations on the material wear and tear of the fast-acting valve. Recently, researchers at the University of Maryland^{138,155} opted to develop a high-enthalpy hypersonic short-duration tunnel by coupling the free-piston and Ludwig tube with a fast-acting valve. The facility can reach Mach numbers between 5 to 7 with a temperature of 1600-1800 K. Many of the existing free-piston or Ludwig facilities that study scramjet engines at high-enthalpy¹⁵⁶⁻¹⁶⁹ using rupture-diaphragms can be upgraded to fast-acting valves for better automation, high repeatability, and clean flow conditions.

Several fast-acting valve concepts have been reported for Ludwig tunnels consolidated in Table V. The fast-acting valve's location in the facility plays a significant role in altering the run time (see Figures 22 and 23). Mounting the valve downstream of the test section ensures a clean and quiet flow upstream. Such a flow field is necessary for studying hypersonic transition-related research. However, the test section is pressurized, and mounting sensors pose difficulties. Ludwig tunnel with a fast-acting valve is helpful for a variety of reasons. Following are some of the significant advantages: 1. simpler construction, 2. easy to automate operations and instrumentation, 4. ensuring remote operations and enhanced safety protocol, 5. lower downtime between successive runs, 6. ability to produce moderate to high enthalpy, 7. economically cheaper compared to other aerodynamic facilities, 8.

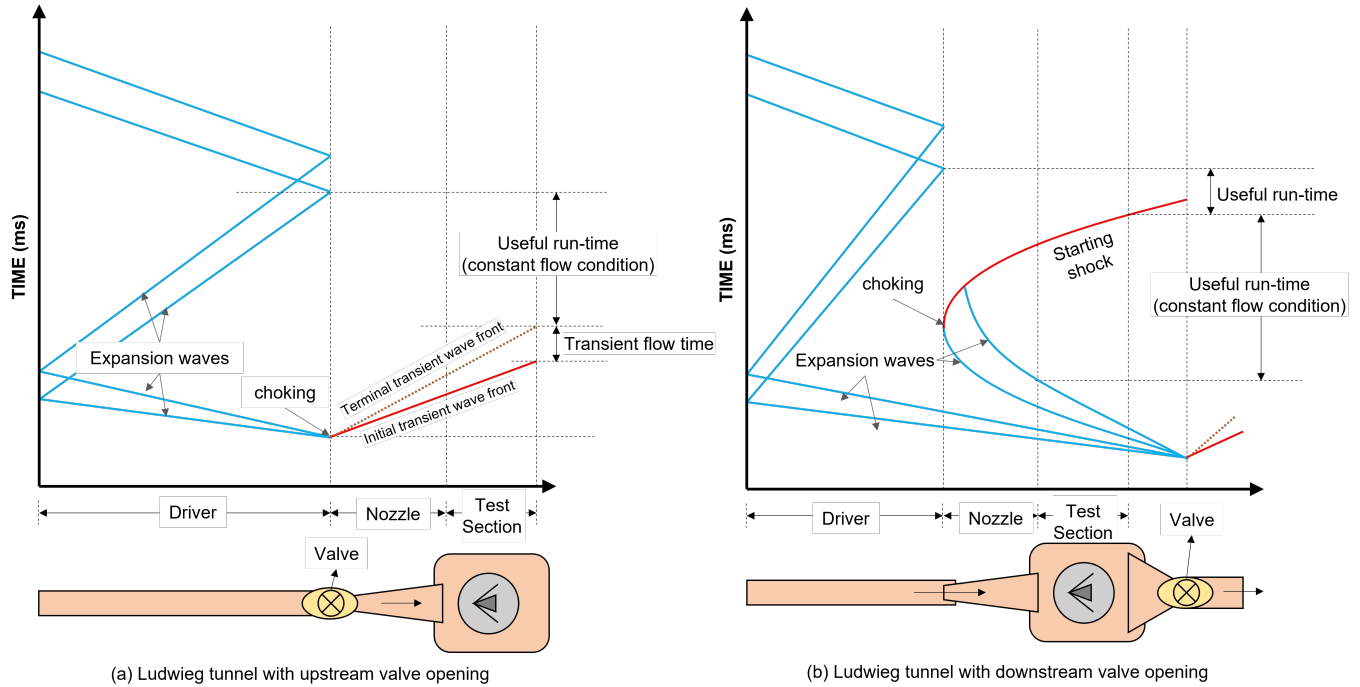


FIGURE 23. Typical trajectory of shock wave, interface, and expansion fans across the different segments of a hypersonic Ludwig tunnel at two different operational mode: (a) upstream and (b) downstream placement of the fast-acting valve. The $x-t$ diagram indicates the attainment of useful run-time obtained during a test, typically on the order of milliseconds (ms).

TABLE V. Some of the Ludwig tube/tunnel type aerodynamic testing facilities that use fast-acting/diaphragmless valves and some vital design parameters^a.

Location ^b	d_m (mm)	Valve Configuration ^c	t_{op} (ms)	t_{ft} (ms)	T_0 (K)	p_0 (bar)	M
TUB, Germany ^{15,46,126-130}	200	Type-II(a):U	23	80	500	3-30	3-6
UB, Germany ¹³¹	-	Type-II(a):U	-	80-130	900	100	11
ZARM-UB, Germany ¹³²	336	Type-II(a):U	-	120	1000	50	<1
DLR, Germany ¹³³⁻¹³⁵	800	Type-II(c):D	-	100-1000	105	12.5	0.3-0.95
UTA, USA ¹³⁶	353	Type-II(c):D	65	120	300	45	0.5-1.2
AFRL, USA ¹³⁷	247.65	Type-II(a):U	20	80	500	7-27	6
UM, USA ¹³⁸	-	Type-II(a):U	~5	100	1600-1800	60	6
USFA, USA ^{139,140}	247.65	Type-II(a):U	≤15	100	300-673	10-40	6
USQ, Australia ¹⁴¹⁻¹⁴⁵	247.65	Type-II(a):U	≤15	100	300-673	10-40	6
DUT, The Netherlands ¹⁴⁶	40	Type-II(a):U	2.1-9	-	573	1-8.5	-
DUT, The Netherlands ¹⁴⁷	49.25-59	Type-II(a):U	10	100	579	2.2-88	6.4 10.5
KAU, Saudi Arabia ^{148,149}	394.4	Type-II(c):D	10-17	95	300	2-20	1.9
KU, Japan ¹⁵⁰	60	RO gate-valve:D	10-17	30	300	3	2-4
IISc, India ^{151,152}	50	Type-II(a):U	10	35	300	10-40	8
Technion-IIT, Israel ^{153,154}	25	Type-II(a):U	≤1	12.5	300-500	2-10	6

^a Values are gathered from the published literature, and official websites of the testing facilities. Some values are not available directly in the literature and they are left unfilled. Nomenclature: d_m -mounting tube diameter, t_{op} -valve opening time, t_{ft} -flow test time, T_0 -stagnation temperature, p_0 -stagnation pressure, M_∞ -freestream Mach number

^b TUB-Technical University of Braunschweig, UB-University of Bremen, ZARM-Center of Applied Space Technology and Microgravity (in English), DLR-German Aerospace Center (in English), UTA-University of Texas at Arlington, AFRL-Air Force Research Laboratory, UM-University of Maryland (under construction), USFA-United States Air Force Academy, DUT-Delft University of Technology, KAU-King Abdulaziz University, KU-Kyushu University, IISc-Indian Institute of Science, IIT-Israel Institute of Technology.

^c U-upstream and D-downstream of the test-section, RO-rapid opening.

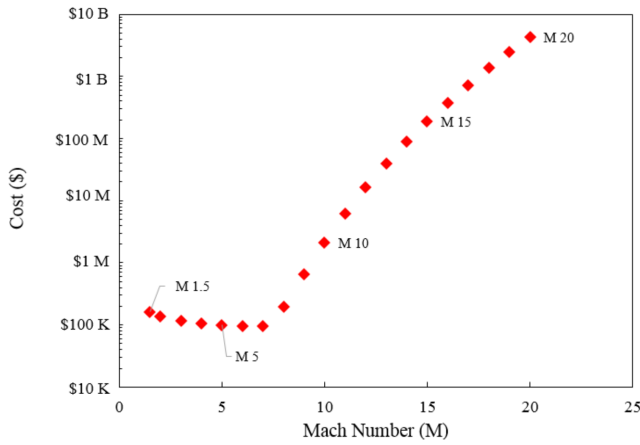


FIGURE 24. Cost analysis proposed by Eugene and Combs¹⁷⁰ for their newly commissioned Ludwig tube of a particular test-section configuration and exhaust conditions (Reprinted with permission from Eugene and Combs¹⁷⁰).

repeatability of flow conditions for statistical consistency, 9. reduced turbulence intensity levels, and 10. quiet upstream conditions.

The report of Eugene and Combs¹⁷⁰ easily highlights the effect of cost requirements in Ludwig type of facilities, either with diaphragm or fast-acting valves. A typical cost analysis graph for the present-day Ludwig facility from their work is shown in Figure 24. A typical Ludwig tunnel construction for $M_\infty = 6$ costs only about 97,000 to 122,000 USD (excluding vacuum pump, tank and instrumentation) which runs for about 75 ms. On the other hand, from the archives of NASA history¹⁷¹, a typical construction of a moderate hypersonic blow-down wind tunnel of a similar Mach number with considerable run time was estimated to be around 30 million USD in 1949 itself. After excluding instrumentation costs, while using the commercially available Russian fast-acting valve ISTA[®] KB-20-10, the complete construction of a typical hypersonic Ludwig tunnel (75 mm diameter open jet test-section, $M_\infty = 6$, and $t_r = 12.5$ ms) is estimated to cost about 30,000 USD.

Regarding automation of the Ludwig tunnel, the ease of assembly and operation is vividly shown in Figure 11 of Eugene *et al.*¹⁷². The low volume of high-pressure tubes and the relatively low run time reduce the operational risk in Ludwig tunnels. Besides, advanced optical diagnostics use laser-based systems in addition to the existing high acquisition rate pressure sensors, which require proper timing to repeatedly sample the data during the desired part of the run time. Given the fast-acting valve replacing the diaphragm, almost continuous repeatable bursts are ensured from a remote operating location after proper automation.

The initial performance studies of the AFRL Ludwig tunnel by Kimmel *et al.*¹³⁷ highlight the ability of the tunnel to produce fairly consistent flow conditions as shown in Figure 25. Diaphragms often produce transient flows as they are shredded into pieces during the rupture. The short times are sometimes 10-20% of the whole run time itself and compen-

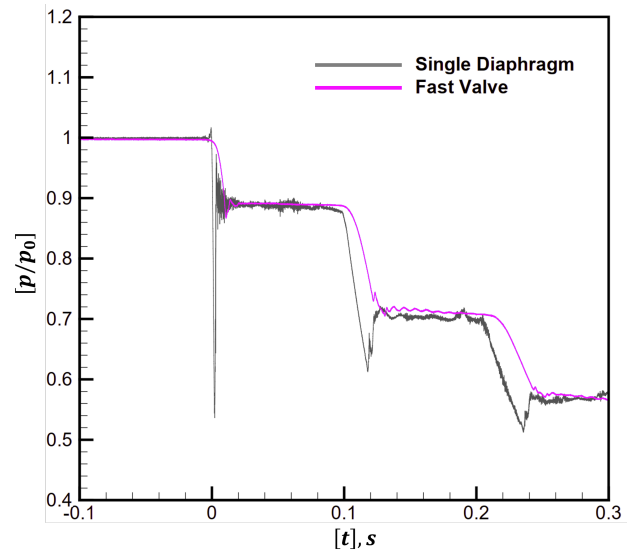


FIGURE 25. A typical run time captured signal captured by monitoring the driver tube pressure while using the diaphragm and fast-acting valve as reported in the work of Kimmel *et al.*¹³⁷ (Reprinted with permission from AIAA: Kimmel *et al.*¹³⁷, copyright 2017). The x-axis represents the time in seconds, and the y-axis represents the dimensionless pressure, where p_0 is the initial driver pressure.

sate for efficient data acquisition. On the other hand, fast-acting valves reduce the transient times by order and offer consistency during repeated runs. In short-duration facilities like the Ludwig tunnels, repeatability is important as the tunnels run times are small enough for advanced optical diagnostics to collect turbulent flow statistics.

The usefulness of the flow quality during the test-time can be appreciated while comparing the usage of a paper diaphragm and a fast-acting valve in a Ludwig tunnel. For simple pitot measurements on a flat-disc, the standing shock should be stationary for an unsteady flow. If the flow has free disturbances from the non-uniform breaking of the diaphragm or its chunks, then the standing shock is no longer stationary but oscillates. In the Schlieren image shown in Figure 26a, the paper diaphragm enters the test-section during the test-time and contaminates the flow to a greater extent. The shock is completely unsteady, and the oscillations can be seen in the $x-t$ diagram shown in Figure 26b. On the other hand, while using the fast-acting valve, the flow is steady (Figure 26c). The $x-t$ diagram shows the achieved useful steady test-time, marked by the presence of the detached shock as a solid vertical line.

D. Precise calibration of sensors

Dynamic calibration of pressure sensors using shock tubes is a notable method due to their inherent capability to generate pressure pulses of desired amplitude and fast rise time^{173,174}. The amplitude of step jump in pressure can be analytically calculated using the well-known shock tube relations. The pressure jump, P_{51} , behind the reflected shock wave in a shock

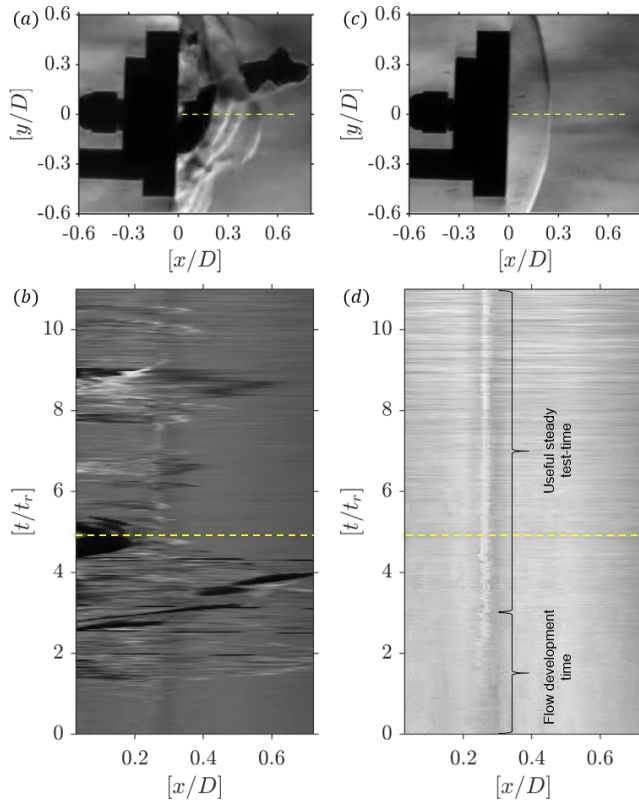


FIGURE 26. Instantaneous schlieren imaging showing (a) the influence of the paper diaphragm in the flow field and (c) a clean flow with a steady detached shock (flow is from right to left at a freestream Mach number of $M_\infty=6$). The respective $x-t$ diagrams constructed by piling up the intensity variation along the dotted yellow line at each time instants along the center for (a) and (c) is shown in (b) and (d). The y -axis represents the dimensionless time, where t_r is a reference time of 1 ms, and the x -axis represents the dimensionless spatial units, where D is the diameter of the disc. The dotted yellow line particularly in (c) and (d) mark the respective time instant in which the instantaneous images (a) and (c) are taken.

tube is given by,

$$P_{51} = \left[\frac{2\gamma_1 M_S^2 - (\gamma_1 - 1)}{\gamma_1 + 1} \right] \left[\frac{(3\gamma_1 - 1)M_S^2 - 2(\gamma_1 - 1)}{(\gamma_1 - 1)M_S^2 + 2} \right] \quad (21)$$

where γ is the specific heat ratio, M_S is the incident shock Mach Number. Svete et al.'s method characterizes the dynamic performance of pressure transducers with a relative expanded uncertainty of less than 0.025^{94,95}. Their diaphragmless shock tube has the potential to be a primary time-varying pressure calibration standard to generate pressure steps with the desired magnitude. Experiments in the diaphragmless shock tube with a commercial fast-acting valve were performed for pressure steps with magnitudes ranging from approximately 0.83 MPa to 1.32 MPa. Sembian et al.'s novel technique using converging shock waves pushed the upper limit of the calibration to medium-high pressure range as there is an increasing need for a traceable dynamic calibration standard across wider pressure ranges⁹⁶. Using the converging shock waves technique, pressure pulses with peak amplitudes

in the range of 30–40 MPa, with < 3.4% uncertainty based on numerical reference profile, were realized.

E. Novel industrial applications

Diaphragmless shock tubes have been used for a variety of novel industrial applications. Miyachi et al.'s diaphragmless driver was an attempt to address the environmental destruction of the marine ecosystem caused by micro-organisms in ship ballast water⁶⁵. The basic idea was to kill marine bacteria in a large amount of ballast water by treating it with strong pressure pulses and free radicals created from the collapse of microbubbles. The work on ballast water treatment was extended to the rapid-opening valve developed by Abe et al.⁶⁶. The pneumatic-cylinder-based diaphragmless shock tube proposed by Hariharan et al. was designed for a variety of industrial applications⁶⁹. The most notable application was the sandal oil extraction enhancement using the diaphragmless shock tube⁷. The rate and quantity of oil extracted from the sandalwood specimen exposed to shock waves were higher than conventional methods¹⁷⁵. The amount of oil extracted in different sandalwood samples after shock wave loading showed an increase of 4.56 – 58.51% compared to the oil extracted from samples not exposed to shock waves. The rate of oil extraction in the samples exposed to shock waves was substantially enhanced during the initial 30 min of the extraction process compared to nondestructive oil extraction techniques.

F. Miscellaneous applications

Diaphragmless shock tubes have been used to study shock-induced deformation of metals like aluminum, copper, and brass^{176–178}. Precise control over the driver pressure and repeatable shock conditions are specific advantages of using diaphragmless shock tubes in these studies. Fast-acting valves have been used for other combustion applications apart from shock tubes. As an example, a fast-acting pneumatic valve was developed for injecting hydrogen into the combustion chamber of a scramjet (supersonic combustion ramjet) engine model¹⁷⁹. This valve had an adjustable opening time with a minimum value of 10 ms. Although a commercial solenoid valve could achieve these opening times easily, customized fast-acting valve was designed to meet the space restrictions. This valve has been used for injection applications in a number of studies in transient shock tunnels^{162,180,181}. Shock waves have been extended to biological and biomedical engineering research in recent years¹⁸². Shock tubes have been used as blast simulators to study blast-induced neurotrauma in laboratory scales. Precise control over the repeatability of pressure pulses is essential while working with biological samples. Diaphragm fragments propagating with the flow can contaminate and sometimes even be detrimental to biological samples placed at the end of the shock tube. These drawbacks are overcome by using diaphragmless shock tubes to produce low-intensity shock waves. The table-top diaphragmless shock tube developed by Swietek et al. for traumatic

brain injury (TBI) studies is an economical and safe alternative to using conventional shock tubes⁹³. Teshima's vertical diaphragmless shock tube was used to study biomechanical and biological effects of high-pressure pulses on microorganisms and DNA⁵⁹. The facility could produce shock waves with an amplitude of 10 MPa, and a pulse width of about 25 microseconds at high repetition. Divya Prakash et al., for the first time, performed an *in vivo* study of shock wave treatment of biofilms in a murine model using 50 mm diaphragmless shock tube¹⁸³. In combination with antibiotic therapy, the studies showed that shock waves could treat lung and skin infections caused by bacteria.

VIII. CONCLUDING REMARKS AND FUTURE SCOPE

Using fast-acting valves in shock tubes presents many advantages over the conventional mode of operation. The various diaphragmless driver designs developed over the last half-century have been compiled and discussed in detail in this review. Critical design features like the type of closure element, actuators, control parameters, driver-driven configurations, and valve opening time are explained. The following conclusions can be drawn from this review:

- The opening time of the fast-acting valve is a vital parameter that determines the shock wave parameters obtained at the end of the shock tube. The opening time in fast-acting valves reported to date cannot match the time-scale of a diaphragm rupture. At higher pressure ratios (P_{41}), the deviation of the shock Mach number is significant as compared to the diaphragm-type mode of operation.
- The shock formation distance is directly proportional to the opening time of the fast-acting valve. Diaphragmless shock tubes have longer shock formation distances than diaphragm-type shock tubes; therefore, longer driven sections are required.
- The efficiency of a diaphragmless driver is comparable to a diaphragm-type mode of operation at lower pressure ratios ($P_{41} \leq 50$).
- Lighter closure elements are preferable in fast-acting valves. A cap made of high-strength composites is a good choice for faster retraction and a wide operating range.
- Pneumatic or electro-pneumatic actuators have fast action over long stroke movement of closure elements compared to hydraulic and purely electrical actuators.
- Inline mounting of the driver and driven sections in diaphragmless shock tubes is a desirable configuration because of its closeness to replicating the wave system in a conventional shock tube and the ease of converting existing conventional shock tubes to diaphragmless shock tubes.

A mathematical model to describe the motion of the closure element in the fast-acting valve has been developed and presented. The versatility of diaphragmless shock tubes as a reliable high-temperature wave reactor, an automated aerodynamic test facility, a precise pressure calibration standard, a tool for biological research, and disruptive technology for innovative industrial applications has been illustrated with several examples.

The design improvement of paramount importance in diaphragmless shock tubes is to shorten the opening time of fast-acting valves without inducing undesirable flow features in the shock tube. Advances in actuation technology promise more robust and compact actuators to realize quicker opening times in the future. Nevertheless, diaphragmless shock tubes in the present development stage provide limitless opportunities for applications in untapped interdisciplinary fields of science and technology. Novel applications of shock tubes are being demonstrated in material synthesis and modification, food preservation and quality enhancement, cell transformation, gene therapy, wound healing, etc. With these areas of shock wave applications being continuously explored, diaphragmless shock tubes have a very important role for many years.

ACKNOWLEDGMENTS

The work of authors from King Abdullah University of Science and Technology (KAUST) was funded by the baseline research funds at KAUST.

REFERENCES

- ¹G. Ben-Dor, O. Igra, and T. Elperin, *Handbook of shock waves, three volume set* (Elsevier, 2000).
- ²J. N. Bradley, *Shock waves in chemistry and physics* (Methuen, 1962).
- ³A. G. Gaydon and I. R. Hurler, *The shock tube in high-temperature chemical physics* (Reinhold Publishing Corporation, 1963).
- ⁴K. Takayama, "Shockwave/geophysical and medical applications," *Annual Review of Fluid Mechanics* **36**, 347–379 (2004).
- ⁵K. Takayama, "Summary of forty years continuous shock wave research at interdisciplinary shock wave research center, tohoku university," in *Shock Waves* (Springer, 2005) pp. 3–10.
- ⁶K. Takayama and K. Ohtani, "Applications of shock wave research to medicine," *WIT Transactions on Modelling and Simulation* **41** (2005).
- ⁷G. Jagadeesh, "Industrial applications of shock waves," *Proceedings of the Institution of Mechanical Engineers, Part G: Journal of Aerospace Engineering* **222**, 575–583 (2008).
- ⁸G. Jagadeesh, "Application of shock waves in pencil manufacturing industry," in *Shock Waves* (Springer, 2009) pp. 847–850.
- ⁹T. Bolumar, M. Enneking, S. Toepfl, and V. Heinz, "New developments in shockwave technology intended for meat tenderization: Opportunities and challenges. a review," *Meat Science* **95**, 931–939 (2013).
- ¹⁰L. E. Murr, *Shock waves for industrial applications* (Park Ridge, NJ (US); Noyes Publications, 1988).
- ¹¹G. F. Kinney and K. J. Graham, *Explosive shocks in air* (Springer Science & Business Media, 2013).
- ¹²M. N. Director and E. K. Dabora, "An experimental investigation of variable energy blast waves," *Acta Astronautica* **4**, 391–407 (1977).

- ¹³H. Honma, I. Glass, C. Wong, O. Holst-Jensen, and D. Xu, "Experimental and numerical studies of weak blast waves in air," *Shock Waves* **1**, 111–119 (1991).
- ¹⁴W. Bleakney, D. Weimer, and C. Fletcher, "The shock tube: a facility for investigations in fluid dynamics," *Review of Scientific Instruments* **20**, 807–815 (1949).
- ¹⁵A. Wagner, E. Schülein, R. Petervari, K. Hannemann, S. R. C. Ali, A. Cerninara, and N. D. Sandham, "Combined free-stream disturbance measurements and receptivity studies in hypersonic wind tunnels by means of a slender wedge probe and direct numerical simulation," *Journal of Fluid Mechanics* **842**, 495–531 (2018).
- ¹⁶B. R. Capra, R. R. Boyce, M. Kuhn, and H. Hald, "Combustion enhancement in a scramjet engine using oxygen enrichment and porous fuel injection," *Journal of Fluid Mechanics* **767**, 173–198 (2015).
- ¹⁷S. R. Nagaraja, J. K. Prasad, and G. Jagadeesh, "Theoretical–experimental study of shock wave-assisted metal forming process using a diaphragmless shock tube," *Proceedings of the Institution of Mechanical Engineers, Part G: Journal of Aerospace Engineering* **226**, 1534–1543 (2011).
- ¹⁸V. Jayaram, S. Preetam, and K. P. J. Reddy, "Experimental investigation of nano ceramic material interaction with high enthalpy argon under shock dynamic loading," *Applied Mechanics and Materials* **83**, 66–72 (2011).
- ¹⁹R. Condit, "The shock-wave valve," in *December meeting of the American Physical Society* (American Physical Society, 1954) pp. 945–945.
- ²⁰O. E. Kosing, F. J. Barbosa, and B. W. Skews, "A new, friction controlled, piston actuated diaphragmless shock tube driver," *Shock Waves* **9**, 69–72 (1999).
- ²¹R. Mejia-Alvarez, B. Wilson, M. C. Leftwich, A. A. Martinez, and K. P. Prestridge, "Design of a fast diaphragmless shock tube driver," *Shock Waves* **25**, 635–650 (2015).
- ²²W. S. McGivern, I. A. Awan, and J. A. Manion, "Diaphragmless single-pulse shock tube for high-temperature chemical kinetics studies," *Rev Sci Instrum* **90**, 064101 (2019).
- ²³T. Ikui, K. Matsuo, and Y. Yamamoto, "Fast-acting valves for use in shock tubes : Part 2, formation of shock waves," *Bulletin of JSME* **22**, 693–699 (1979).
- ²⁴R. Becker, "Stosswelle und detonation," *Zeitschrift für Physik* **8**, 321–362 (1922).
- ²⁵T. Ikui, K. Matsuo, and Y. Yamamoto, "Fast-acting valves for use in shock tubes: part 1, construction and their characteristics," *Bulletin of JSME* **20**, 337–342 (1977).
- ²⁶S. Janardhanraj, K. Abhishek, and G. Jagadeesh, "Insights into the shock-wave attenuation in miniature shock tubes," *Journal of Fluid Mechanics* **910** (2021).
- ²⁷P. Gaetani, A. Guardone, and G. Persico, "Shock tube flows past partially opened diaphragms," *Journal of Fluid Mechanics* **602**, 267–286 (2008).
- ²⁸T. T. N. Nguyen, J. M. Wilgeroth, and W. G. Proud, "Controlling blast wave generation in a shock tube for biological applications," *18th Aps-Scem and 24th Airtap, Pts 1-19* **500** (2014), 10.1088/1742-6596/500/14/142025.
- ²⁹A. Tulgestke, S. Johnson, D. Davidson, and R. Hanson, "High-speed imaging of inhomogeneous ignition in a shock tube," *Shock Waves* **28**, 1089–1095 (2018).
- ³⁰D. R. White, "Influence of diaphragm opening time on shock-tube flows," *Journal of Fluid Mechanics* **4**, 585–599 (1958).
- ³¹E. Rothkopf and W. Low, "Diaphragm opening process in shock tubes," *The Physics of Fluids* **17**, 1169–1173 (1974).
- ³²J. de Souza Vianna, A. de Souza Oliveira, and J. Damion, "Influence of the diaphragm on the metrological characteristics of a shock tube," *Metrologia* **36**, 599 (1999).
- ³³R. S. Hickman, L. C. Farrar, and J. B. Kyser, "Behavior of burst diaphragms in shock tubes," *Physics of Fluids* **18** (1975), 10.1063/1.861010.
- ³⁴M. Brouillette, "Shock waves at microscales," *Shock waves* **13**, 3–12 (2003).
- ³⁵I. d. S. RÊGo, K. Sato, Y. Miyoshi, T. Ando, K. Goto, M. Sakamoto, S. Kawasaki, and T. E. Group, "A newly developed large diameter diaphragmless shock tube for studies on co₂-n₂ gas-dynamic laser," *Plasma and Fusion Research* **2**, 033–033 (2007).
- ³⁶J. Bradley, R. Butlin, and J. Quinn, "An electrical method for breaking shock tube diaphragms," *Journal of Scientific Instruments* **42**, 901 (1965).
- ³⁷A. L. Cole, A. C. Hunting, D. L. Upham, and O. Laporte, "Electrical breaking of shock-tube diaphragms: progress report," Tech. Rep. (University of Michigan, Ann Arbor, 1958).
- ³⁸A. Roshko and D. Baganoff, "A novel device for bursting shock-tube diaphragms," *Physics of Fluids* **4** (1961), 10.1063/1.1706238.
- ³⁹B. W. Skews and T. O. Duggan, "Gas-operated diaphragm clamp for a shock tube," *Review of Scientific Instruments* **39**, 1063–1064 (1968).
- ⁴⁰I. Stotz, G. Lamanna, H. Hettrich, B. Weigand, and J. Steelant, "Design of a double diaphragm shock tube for fluid disintegration studies," *Review of Scientific Instruments* **79**, 125106 (2008).
- ⁴¹J. C. Muirhead and W. A. Jones, "Shock wave valves," *Review of Scientific Instruments* **35**, 119–120 (1964).
- ⁴²H. Oguchi, K. Funabiki, and S. Sato, "An experiment on interaction of shock wave with multiple-orifice plate by means of snap-action shock tube," *Modern Developments in Shock Tube Research*, 386–391 (1975).
- ⁴³E. Distéfano and N. Fraidenaich, "An electromagnetic diaphragm for use in shock tubes," *Review of Scientific Instruments* **41**, 886–887 (1970).
- ⁴⁴H. Oguchi, K. Funabiki, and S. Sato, "A new type of shock valve and its characteristic performance," *University of Tokyo, ISAS RN* **20** (1976).
- ⁴⁵T. Ikui, K. Matsuo, and Y. Yamamoto, "Study of a quick opening valve for shock tube research, part 1 structure and characteristics," *Trans. JSME B* **42**, 2127–2132 (1976).
- ⁴⁶O. Igra and F. Seiler, *Experimental methods of Shock wave research*, Vol. 478 (Springer, 2016).
- ⁴⁷W. Garen, R. Synofzik, and A. Frohn, "Shock tube for generating weak shock waves," *AIAA Journal* **12**, 1132–1134 (1974).
- ⁴⁸K. Matsuo, S. Kawagoe, T. Ogawara, and H. Tsubaki, "Modern developments in shock tube research," in *Proceedings of 10th Int. Shock Tube Symp* (1975) p. 265.
- ⁴⁹K. Takayama, "The shock wave and beyond, a tribute to professor glass," in *Professor II Glass: A Tribute and Memorial* (Springer, 2013) pp. 7–109.
- ⁵⁰E. Timofeev, K. Takayama, P. Voinovich, E. Timofeev, K. Takayama, and P. Voinovich, "Numerical and experimental observation of three-dimensional unsteady shock wave structures," in *35th Aerospace Sciences Meeting and Exhibit* (1997) p. 70.
- ⁵¹K. Maeno, "Shock wave propagation in low temperature fluids and phase change phenomena," in *Adiabatic Waves in Liquid-Vapor Systems*, edited by G. E. A. Meier and P. A. Thompson (Springer Berlin Heidelberg, Berlin, Heidelberg, 1990) pp. 69–78.
- ⁵²H. Oguchi, K. Funabiki, T. Sato, and K. Maeno, "An experimental study on co₂ gasdynamic laser by means of non-diaphragm shock tubes," *Report of Institute of Space and Astronautical Science, University of Tokyo* **14**, 809–829 (1978).
- ⁵³K. Maeno, K. Funabiki, and H. Oguchi, "Experimental and analytical study of co₂/n₂ mixing gasdynamic laser," *Tokyo University Institute of Space and Aeronautical Science Report* **46**, 175–197 (1981).
- ⁵⁴K. Maeno and H. Oguchi, "Study on n₂/co₂ mixing gasdynamic laser by means of synchronized operation of two shock tubes," *Le Journal de Physique Colloques* **41**, C9–209–C9–215 (1980).
- ⁵⁵M. Yamauchi, H. Matsui, M. Koshi, K. Tanaka, S. Tamaki, and H. Tanaka, "Shock tube studies on the radical emission spectra by use of an imaging spectrometer," *Journal of the Spectroscopical Society of Japan* **36**, 388–394 (1987).
- ⁵⁶S. M. Hurst and S. H. Bauer, "A piston-actuated shock-tube, with laser-schlieren diagnostics," *Review of Scientific Instruments* **64**, 1342–1346 (1993).
- ⁵⁷H. Matsui, M. Koshi, M. Oya, and K. Tsuchiya, "Improvement of chemical kinetic data at high temperatures by piston actuated shock tube, excimer laser photolysis, and atomic resonance absorption spectrometry," *Shock Waves* **3**, 287–292 (1994).
- ⁵⁸Y. Takano and T. Akamatsu, "A diaphragmless shock tube," *Journal of Physics E: Scientific Instruments* **17**, 644 (1984).
- ⁵⁹K. Teshima, "High-frequency generation of high-pressure pulses using a diaphragmless shock tube," in *Shock Waves@ Marseille I* (Springer, 1995) pp. 221–226.
- ⁶⁰I. da S. Rego, K. N. Sato, S. Kugimiya, T. Aoki, Y. Miyoshi, T. Ando, K. Goto, and M. Sakamoto, "Development of a large diameter diaphragmless shock tube for gas-dynamic laser studies," *Materials Science Forum* **566**, 9–14 (2007).

- ⁶¹H. Onodera, "Double piston shock-wave valve," *AIAA Journal* **30**, 2569–2571 (1992).
- ⁶²M.-Y. Zhang, X. Chen, P. Liu, K.-D. Yang, and H.-D. Zhu, "Design of diaphragmless shock tube and research on its normal temperature characteristics," *Journal of Physics: Conference Series* **1601**, 062018 (2020).
- ⁶³M. Watanabe, O. Onodera, and K. Takayama, "Shock wave focusing in a vertical annular shock tube," in *Shock Waves@ Marseille IV* (Springer, 1995) pp. 99–104.
- ⁶⁴H. Ojima, K. Kitagawa, M. Kainuma, T. Ogawa, K. Takahashi, M. Sun, and K. Takayama, "Characteristics of a 60mm χ 150mm vertical diaphragmless shock tube," in *23rd International Symposium on Shock Waves* (Fort Worth, USA, 2001).
- ⁶⁵A. Miyachi, K. Sugahara, and A. Abe, "High speed opening operation of diaphragmless shock wave generator," in *28th International Symposium on Shock Waves* (Springer, 2012) pp. 711–717.
- ⁶⁶A. Abe, K. Sugahara, and Y. Yamada, "Rapid opening valve assisted by magnetic force for a diaphragmless shock tube," in *29th International Symposium on Shock Waves 1* (Springer, Cham, 2015) Book section Chapter 52, pp. 337–342.
- ⁶⁷T. Abe, E. Ogura, S. Sato, and K. Funabiki, "Rupture-disk-less shock-tube with compression tube driven by free piston," *Shock Waves* **7**, 205–209 (1997).
- ⁶⁸M. Bredin and B. Skews, "Drag measurement in unsteady compressible flow—part 1: An unsteady flow facility and stress wave drag balance," *RD J. South Afr. Inst. Mech.* **23**, 1–10 (2007).
- ⁶⁹M. S. Hariharan, S. Janardhanraj, S. Saravanan, and G. Jagadeesh, "Diaphragmless shock wave generators for industrial applications of shock waves," *Shock Waves* **21**, 301–306 (2010).
- ⁷⁰M. Taguchi, M. Kashitani, and M. Nishiyama, "Fundamental study on operational conditions of diaphragmless shock tube driven by pneumatic piston," *International Journal of Mechanical Engineering and Robotics Research* **7** (2018).
- ⁷¹M. Nishiyama, M. Taguchi, and M. Kashitani, "Fundamental study on operational parameters of diaphragmless shock tube," in *MATEC Web of Conferences*, Vol. 151 (EDP Sciences, 2018) p. 02004.
- ⁷²S. Itahashi, T. Meguro, O. Onodera, H. Ojima, T. Ogawa, and K. Takayama, "Characteristics of a 100 mm x 180 mm diaphragmless shock tube using a piston quick opening valve," *Proc of Symp on Shock Waves*, Tokyo, Japan , 211 (1996).
- ⁷³J. Yang, O. Onodera, and K. Takayama, "Design and performance of quick opening shock tube using rubber membrane for weak shock wave generation," *JSME B* **60**, 473–478 (1994).
- ⁷⁴R. S. Tranter and B. R. Giri, "A diaphragmless shock tube for high temperature kinetic studies," *Rev Sci Instrum* **79**, 094103 (2008).
- ⁷⁵S. Udagawa, W. Garen, B. Meyerer, and K. Maeno, "Interferometric detection of dispersed shock waves in small scale diaphragm-less shock tube of 1mm diameter," 16th Australasian Fluid Mechanics Conference (AFMC) (2007).
- ⁷⁶W. Garen, B. Meyerer, S. Udagawa, and K. Maeno, "Shock waves in minitubes: influence of the scaling parameter s," *Shock Waves, Vol 2, Proceedings* , 1473–+ (2009).
- ⁷⁷S. Udagawa, W. Garen, B. Meyerer, and K. Maeno, "Motion analysis of a diaphragmless driver section for a narrow channel shock tube," *Shock Waves* **18**, 345–351 (2008).
- ⁷⁸S. Udagawa, K. Maeno, I. Golubeva, and W. Garen, "Interferometric signal measurement of shock waves and contact surfaces in small scale shock tube," *Shock Waves, Vol 2, Proceedings* , 1419–+ (2009).
- ⁷⁹H. R. Hosseini, O. Onodera, and K. Takayama, "Stability of converging cylindrical shock waves in a vertical annular co-axial diaphragmless shock tube," *Transactions of the Japan Society for Aeronautical and Space Sciences* **42**, 19–26 (1999).
- ⁸⁰S. H. R. Hosseini, O. Onodera, and K. Takayama, "Characteristics of an annular vertical diaphragmless shock tube," *Shock Waves* **10**, 151–158 (2000).
- ⁸¹Y. W. Kim, "A new diaphragmless shock tube facility for interface instability and mach reflection studies," in *Shock Waves@ Marseille I* (Springer, 1995) pp. 227–232.
- ⁸²J. B. Randazzo and R. S. Tranter, "Note: An improved driver section for a diaphragmless shock tube," *Rev Sci Instrum* **86**, 016117 (2015).
- ⁸³S. Shiozaki, I. Kinefuchi, Y. Sakiyama, S. Takagi, and Y. Matsumoto, "Development of high energy molecular beam source using small shock tube," *Rarefied Gas Dynamics* **762**, 875–879 (2005).
- ⁸⁴K. Heufer, H. Olivier, S. Drumm, and H. Murrenhoff, "A new fast acting valve for diaphragmless shock tubes," in *28th international symposium on shock waves* (Springer, 2012) pp. 535–540.
- ⁸⁵M. S. Downey, T. J. Cloete, and A. D. B. Yates, "A rapid opening sleeve valve for a diaphragmless shock tube," *Shock Waves* **21**, 315–319 (2011).
- ⁸⁶S. Udagawa, M. Ota, and K. Maeno, "Propagation characteristics of the shock wave in small diameter tubes at atmospheric initial driven pressure," in *28th International Symposium on Shock Waves* (Springer, 2012) pp. 529–534.
- ⁸⁷S. Udagawa, Y. Hirose, W. Garen, T. Inage, M. Ota, and K. Maeno, "Improvement of a diaphragmless driver section for a small diameter shock tube," in *29th International Symposium on Shock Waves 1* (Springer, Cham, 2015) Book section Chapter 53, pp. 343–348.
- ⁸⁸M. E. Fuller, M. Skowron, R. S. Tranter, and C. F. Goldsmith, "A modular, multi-diagnostic, automated shock tube for gas-phase chemistry," *Rev Sci Instrum* **90**, 064104 (2019).
- ⁸⁹J. Subburaj, T. A. Kashif, and A. Farooq, "Methane and n-hexane ignition in a newly developed diaphragmless shock tube," (2022), [10.48550/arXiv.2208.02306](https://doi.org/10.48550/arXiv.2208.02306).
- ⁹⁰R. S. Tranter and P. T. Lynch, "A miniature high repetition rate shock tube," *Rev Sci Instrum* **84**, 094102 (2013).
- ⁹¹P. T. Lynch, "Note: An improved solenoid driver valve for miniature shock tubes," *Rev Sci Instrum* **87**, 056110 (2016).
- ⁹²R. S. Tranter and T. Sikes, "Solenoid actuated driver valve for high repetition rate shock tubes," *Review of Scientific Instruments* **91**, 056101 (2020), <https://doi.org/10.1063/5.0006010>.
- ⁹³B. Swietek, M. Skotak, N. Chandra, and B. J. Pfister, "Characterization of a controlled shock wave delivered by a pneumatic table-top gas driven shock tube," *Review of Scientific Instruments* **90**, 075116 (2019).
- ⁹⁴A. Svete and J. Kutin, "Characterization of a newly developed diaphragmless shock tube for the primary dynamic calibration of pressure meters," *Metrologia* **57** (2020), [10.1088/1681-7575/ab8f79](https://doi.org/10.1088/1681-7575/ab8f79).
- ⁹⁵A. Svete and J. Kutin, "Diaphragmless shock tube for primary dynamic calibration of pressure meters," *ACTA IMEKO* **9**, 310 (2020).
- ⁹⁶S. Sembian and M. Liverts, "On using converging shock waves for pressure amplification in shock tubes," *Metrologia* **57** (2020), [10.1088/1681-7575/ab7f99](https://doi.org/10.1088/1681-7575/ab7f99).
- ⁹⁷E. Amer, M. Wozniak, G. Jönsson, and F. Arrhen, "Evaluation of shock tube retrofitted with fast-opening valve for dynamic pressure calibration," *Sensors* **21**, 4470 (2021).
- ⁹⁸M. A. Samimi, J. Zamani, and F. Sardarzadeh, "Shock wave pressure and velocity measuring using a novel optic sensor in a newly designed diaphragm-less shock tube," *Experimental Techniques* **45**, 55–66 (2020).
- ⁹⁹P. Skousen, *Valve handbook* (McGraw-Hill, New York, 2011).
- ¹⁰⁰K. Sotoodeh, "Actuator selection and sizing for valves," *SN Applied Sciences* **1**, 1–8 (2019).
- ¹⁰¹S. Pakdaman, M. Garcia, E. Teh, D. Lincoln, M. Trivedi, M. Alves, and C. Johansen, "Diaphragm opening effects on shock wave formation and acceleration in a rectangular cross section channel," *Shock waves* **26**, 799–813 (2016).
- ¹⁰²T. Ikui and K. Matsuo, "Investigations of the aerodynamic characteristics of the shock tubes:(part 1, the effects of tube diameter on the tube performance)," *Bulletin of JSME* **12**, 774–782 (1969).
- ¹⁰³C. Simpson, T. Chandler, and K. Bridgman, "Effect on shock trajectory of the opening time of diaphragms in a shock tube," *The physics of Fluids* **10**, 1894–1896 (1967).
- ¹⁰⁴E. Rothkopf and W. Low, "Shock formation distance in a pressure driven shock tube," *The Physics of Fluids* **19**, 1885–1888 (1976).
- ¹⁰⁵M. F. Campbell, K. G. Owen, D. F. Davidson, and R. K. Hanson, "Dependence of calculated postshock thermodynamic variables on vibrational equilibrium and input uncertainty," *Journal of Thermophysics and Heat Transfer* **31**, 586–608 (2017), <https://doi.org/10.2514/1.T4952>.
- ¹⁰⁶M. F. Campbell, A. M. Tulgestke, D. F. Davidson, and R. K. Hanson, "A second-generation constrained reaction volume shock tube," *Review of Scientific Instruments* **85**, 055108 (2014), <https://doi.org/10.1063/1.4875056>.

- ¹⁰⁷M. F. Campbell, T. Parise, A. M. Tulgestke, R. M. Spearrin, D. F. Davidson, and R. K. Hanson, "Strategies for obtaining long constant-pressure test times in shock tubes," *Shock Waves* **25**, 651–665 (2015).
- ¹⁰⁸I. da S. Rêgo, T. Ando, K. Misumi, T. Miyazaki, S. Nishiyori, K. N. Sato, M. Sakamoto, and S. Kawasaki, "A model of piston sliding process for a double piston-actuated shock tube," *Journal of Fluids Engineering* **130** (2008), 10.1115/1.2903521.
- ¹⁰⁹R. Portaro, H. Nakayama, and H. D. Ng, "Analysis of a quick-acting diaphragmless shock tube driver," in *29th International Symposium on Shock Waves I* (Springer Cham, 2015) Book section Chapter 66, pp. 421–426.
- ¹¹⁰M. Koshi, M. Yoshimura, K. Fukuda, H. Matsui, K. Saito, M. Watanabe, A. Imamura, and C. Chen, "Reactions of n (4 s) atoms with no and h₂," *The Journal of chemical physics* **93**, 8703–8708 (1990).
- ¹¹¹C.-C. Hsiao, Y.-P. Lee, N. S. Wang, J.-H. Wang, and M.-C. Lin, "Experimental and theoretical studies of the rate coefficients of the reaction o (3p)+ hcl at high temperatures," *The Journal of Physical Chemistry A* **106**, 10231–10237 (2002).
- ¹¹²B. R. Giri, J. H. Kiefer, H. Xu, S. J. Klippenstein, and R. S. Tranter, "An experimental and theoretical high temperature kinetic study of the thermal unimolecular dissociation of fluoroethane," *Phys Chem Chem Phys* **10**, 6266–73 (2008).
- ¹¹³R. Shaik, A. Kastengren, R. Tranter, and P. Lynch, "Temporally and spatially resolved x-ray densitometry in a shock tube," *Combustion and Flame* **224**, 136–149 (2021), a dedication to Professor Ronald K. Hanson.
- ¹¹⁴T. Sikes, C. Banyon, R. A. Schwind, P. T. Lynch, A. Comandini, R. Sivaramakrishnan, and R. S. Tranter, "Initiation reactions in the high temperature decomposition of styrene," *Phys. Chem. Chem. Phys.* **23**, 18432–18448 (2021).
- ¹¹⁵C. Banyon, T. Sikes, and R. S. Tranter, "Reactions of propyl radicals: A shock tube–vuv photoionization mass spectrometry study," *Combustion and Flame* **224**, 14–23 (2021), a dedication to Professor Ronald K. Hanson.
- ¹¹⁶J. B. Randazzo, R. Sivaramakrishnan, A. W. Jasper, T. Sikes, P. T. Lynch, and R. S. Tranter, "An experimental and theoretical study of the high temperature reactions of the four butyl radical isomers," *Phys. Chem. Chem. Phys.* **22**, 18304–18319 (2020).
- ¹¹⁷P. T. Lynch, T. P. Troy, M. Ahmed, and R. S. Tranter, "Probing combustion chemistry in a miniature shock tube with synchrotron vuv photo ionization mass spectrometry," *Anal Chem* **87**, 2345–52 (2015).
- ¹¹⁸M. Tao, A. Laich, P. Lynch, and P. Zhao, "On the interpretation and correlation of high-temperature ignition delays in reactors with varying thermodynamic conditions," *International Journal of Chemical Kinetics* **50**, 410–424 (2018).
- ¹¹⁹M. Tao, P. T. Lynch, and P. Zhao, "Kinetic modeling of ignition in miniature shock tube," *Proceedings of the Combustion Institute* **37**, 593–601 (2019).
- ¹²⁰S. Nagaraju, R. S. Tranter, F. E. Cano Ardila, S. Abid, P. T. Lynch, G. A. Garcia, J. F. Gil, L. Nahon, N. Chaumeix, and A. Comandini, "Reprint of: Pyrolysis of ethanol studied in a new high-repetition-rate shock tube coupled to synchrotron-based double imaging photoelectron/photoion coincidence spectroscopy," *Combustion and Flame* **224**, 150–165 (2021).
- ¹²¹H. Oguchi, K. Funabiki, S. Sato, and K. Maeno, "An experimental study on co₂ gasdynamic laser by means of non-diaphragm shock tubes," Report from Institute of Space and Astronautical Science, University of Tokyo **14**, 809–829 (1978).
- ¹²²K. Maeno, "Non-diaphragm shock tube and shock waves in low temperature gases (first report)," *Memoirs of the Muroran Institute of Technology. Science and engineering* **35**, 81–93 (1985).
- ¹²³G. Zhang, I. Lee, T. Hashimoto, T. Setoguchi, and H. Kim, "Experimental study on gas-particle two-phase flows in a micro shock tube," *Journal of Visualization* **20**, 17–29 (2017).
- ¹²⁴G. Zhang, I. I. Lee, T. Hashimoto, T. Setoguchi, and H. D. Kim, "Experimental studies on shock wave and particle dynamics in a needle-free drug delivery device," *Journal of Drug Delivery Science and Technology* **41**, 390–400 (2017).
- ¹²⁵P. T. Lynch and G. Wang, "Chemical thermometry in miniature hrst using 1,1,1-trifluoroethane dissociation," *Proceedings of the Combustion Institute* **36**, 307–314 (2017).
- ¹²⁶M. Estorf, T. Wolf, and R. Radespiel, "Experimental and numerical investigations on the operation of the hypersonic ludwig tube braunschweig," in *5th European Symposium on Aerothermodynamics for Space Vehicles* (2004).
- ¹²⁷T. Wolf, M. Estorf, and R. Radespiel, "Simulation of the time-dependent flow field in the hypersonic ludwig tube braunschweig," in *4th Atmospheric Reentry Vehicles & Systems* (2005).
- ¹²⁸T. Wolf, M. Estorf, and R. Radespiel, "Investigation of the starting process in a ludwig tube," *Theoretical and Computational Fluid Dynamics* **21**, 81–98 (2007).
- ¹²⁹S. Stephan, R. Radespiel, and R. Müller-Eigner, "Propulsive jet simulation in a hypersonic ludwig tunnel," in *Deutscher Luft- und Raumfahrtkongress, Berlin* (2012).
- ¹³⁰S. Stephan, R. Radespiel, and R. Müller-Eigner, "Jet simulation facility using the ludwig tube principle," in *Proceedings of the 5th European Conference for Aerospace Sciences (EUCASTS), Munich, Germany* (2013).
- ¹³¹H. Renken, H. W. Oelze, and H. J. Rath, "Application of a digital high-speed camera and image processing system for investigations of short term hypersonic fluids," in *Digital Solid State Cameras: Designs and Applications*, edited by J. George M. Williams (SPIE, 1998).
- ¹³²P. Rickmers, J.-C. Dittmer, and C. Eigenbrod, "Comparison of experimental and numerical results of the autoignition of n-heptane sprays under machine conditions," *International Journal of Microgravity Science and Application* **25**, 367–370 (2008).
- ¹³³H. Rosemann, E. Stanewsky, and G. Hefer, "The cryogenic ludwig-tube of DLR and its new adaptive wall test section," in *Fluid Dynamics Conference* (American Institute of Aeronautics and Astronautics, 1995).
- ¹³⁴M. Costantini, U. Fey, U. Henne, and C. Klein, "Nonadiabatic surface effects on transition measurements using temperature-sensitive paints," *AIAA Journal* **53**, 1172–1187 (2015).
- ¹³⁵M. Costantini, S. Hein, U. Henne, C. Klein, S. Koch, L. Schojda, V. Ondrus, and W. Schröder, "Pressure gradient and nonadiabatic surface effects on boundary layer transition," *AIAA Journal* **54**, 3465–3480 (2016).
- ¹³⁶T. Balcazar, E. Braun, F. Lu, D. Tran, and D. Wilson, "Refurbishment and testing techniques in a transonic ludwig tunnel," in *49th AIAA Aerospace Sciences Meeting including the New Horizons Forum and Aerospace Exposition* (American Institute of Aeronautics and Astronautics, 2011).
- ¹³⁷R. L. Kimmel, M. P. Borg, J. S. Jewell, K.-Y. Lam, R. D. Bowersox, R. Srinivasan, S. Fuchs, and T. Mooney, "AFRL ludwig tube initial performance," in *55th AIAA Aerospace Sciences Meeting* (American Institute of Aeronautics and Astronautics, 2017).
- ¹³⁸J. D. Chung, R. W. Houim, and S. J. Laurence, "Theoretical and numerical study of a preheated ludwig tube with adiabatic compression," *AIAA Journal* **56**, 3951–3962 (2018).
- ¹³⁹R. Cummings and T. McLaughlin, "Hypersonic ludwig tube design and future usage at the US air force academy," in *50th AIAA Aerospace Sciences Meeting including the New Horizons Forum and Aerospace Exposition* (American Institute of Aeronautics and Astronautics, 2012).
- ¹⁴⁰R. Decker, M. Semper, J. Anthony, and R. M. Cummings, "Starting characteristics of the US air force academy mach 6 ludwig tube," in *45th AIAA Fluid Dynamics Conference* (American Institute of Aeronautics and Astronautics, 2015).
- ¹⁴¹G. M. D. Currao, R. Choudhury, S. L. Gai, A. J. Neely, and D. R. Buttsworth, "Hypersonic transitional shock-wave–boundary-layer interaction on a flat plate," *AIAA Journal* **58**, 814–829 (2020).
- ¹⁴²G. M. D. Currao, L. P. McQuellin, A. J. Neely, S. L. Gai, S. O'Byrne, F. Zander, D. R. Buttsworth, J. J. McNamara, and I. Jahn, "Hypersonic oscillating shock-wave/boundary-layer interaction on a flat plate," *AIAA Journal* **59**, 940–959 (2021).
- ¹⁴³B. Birch, D. Buttsworth, R. Choudhury, and N. Stern, "Characterization of a ludwig tube with free piston compression heating in mach 6 configuration," in *22nd AIAA International Space Planes and Hypersonics Systems and Technologies Conference* (American Institute of Aeronautics and Astronautics, 2018).
- ¹⁴⁴D. Buttsworth and M. Smart, "Development of a ludwig tube with free piston compression heating for scramjet inlet starting experiments," in *48th AIAA Aerospace Sciences Meeting Including the New Horizons Forum and Aerospace Exposition* (American Institute of Aeronautics and Astronautics, 2010).
- ¹⁴⁵D. Buttsworth, "Ludwig tunnel facility with free piston compression heating for supersonic and hypersonic testing," (2010).

- ¹⁴⁶T. Mathijssen, M. Gallo, E. Casati, N. R. Nannan, C. Zamfirescu, A. Guardone, and P. Colonna, "The flexible asymmetric shock tube (FAST): a ludwig tube facility for wave propagation measurements in high-temperature vapours of organic fluids," *Experiments in Fluids* **56** (2015), 10.1007/s00348-015-2060-1.
- ¹⁴⁷F. F. J. Schrijer and W. J. Bannink, "Description and flow assessment of the delft hypersonic ludwig tube," *Journal of Spacecraft and Rockets* **47**, 125–133 (2010).
- ¹⁴⁸K. Juhany and H. Aldakhil, "AT0 ludwig tube wind tunnel at KAU," in *44th AIAA Aerospace Sciences Meeting and Exhibit* (American Institute of Aeronautics and Astronautics, 2006).
- ¹⁴⁹K. A. Juhany and A. Darji, "Force measurement in a ludwig tube tunnel," *Journal of Spacecraft and Rockets* **44**, 88–93 (2007).
- ¹⁵⁰K. Matsuo, S. Kawagoe, and T. Ogawara, "Starting process of a supersonic ludwig tube with a downstream valve," *Bulletin of JSME* **21**, 1610–1617 (1978).
- ¹⁵¹S. M. V. Rao, N. N. H, N. K., and S. S., "Study of the sonic jet from a novel mixing enhancement nozzle in supersonic cross-flow," in *Proceedings of the 32nd International Symposium on Shock Waves (ISSW32 2019)* (Research Publishing Services, 2019).
- ¹⁵²M. I. Sugarno, R. Sriram, S. K. Karthick, and G. Jagadeesh, "Unsteady pulsating flowfield over spiked axisymmetric forebody at hypersonic flows," *Physics of Fluids* **34**, 016104 (2022).
- ¹⁵³"Experiments in a hypersonic miniature ludwig tunnel at different reynolds numbers on a flat-face spiked-body at a freestream mach number of 6," in *The 61st Israel Annual Conference on Aerospace Sciences (IACAS)*, edited by S. K. Karthick, S. R. Nanda, and J. Cohen (2021).
- ¹⁵⁴S. K. Karthick, S. R. Nanda, and J. Cohen, "Unsteadiness in hypersonic leading-edge separation," (2022).
- ¹⁵⁵J. D. Chung, *Quasi-one-dimensional modeling of an adiabatic-compression preheated Ludwieg tube*, Master's thesis, University of Maryland, College Park (2015).
- ¹⁵⁶C. J. Jachimowski, "An analysis of combustion studies in shock expansion tunnels and reflected shock tunnels," Tech. Rep. 3224 (NASA Technical Paper, NASA, 1992).
- ¹⁵⁷J. A. COPPER, "Effects of interface combustion and mixing on shock-tunnel conditions," *AIAA Journal* **2**, 1669–1671 (1964).
- ¹⁵⁸S. Aso, A. N. Hakim, S. Miyamoto, K. Inoue, and Y. Tani, "Fundamental study of supersonic combustion in pure air flow with use of shock tunnel," *Acta Astronautica* **57**, 384–389 (2005).
- ¹⁵⁹A. Paull, R. J. Stalker, and D. J. Mee, "Experiments on supersonic combustion ramjet propulsion in a shock tunnel," *Journal of Fluid Mechanics* **296**, 159–183 (1995).
- ¹⁶⁰R. Stalker, A. Paull, D. Mee, R. Morgan, and P. Jacobs, "Scramjets and shock tunnels—the queensland experience," *Progress in Aerospace Sciences* **41**, 471–513 (2005).
- ¹⁶¹K. Srinivasan, P. K. Maurya, K. Abhishek, S. L. N. Desikan, and B. Murugan, "Supersonic combustion of a scramjet engine using hydrogen fuel in shock tunnel," *AIAA Journal* **56**, 3600–3609 (2018).
- ¹⁶²M. N. Wendt and R. J. Stalker, "Transverse and parallel injection of hydrogen with supersonic combustion in a shock tunnel," *Shock Waves* **6**, 53–59 (1996).
- ¹⁶³R. R. Boyce, A. Paull, R. J. Stalker, M. Wendt, N. Chinzei, and H. Miyajima, "Comparison of supersonic combustion between impulse and vitiation-heated facilities," *Journal of Propulsion and Power* **16**, 709–717 (2000).
- ¹⁶⁴Y. Hongru, "Oxyhydrogen combustion and detonation driven shock tube," *Acta Mechanica Sinica* **15**, 97–107 (1999).
- ¹⁶⁵A. Ben-Yakar and R. K. Hanson, "Characterization of expansion tube flows for hypervelocity combustion studies," *Journal of Propulsion and Power* **18**, 943–952 (2002).
- ¹⁶⁶A. Ridings, *Investigation of pre-combustion shock trains in a sramjet using a shock tunnel at Mach 8 flight conditions*, Ph.D. thesis.
- ¹⁶⁷H. T. Nagamatsu and E. D. Martin, "Combustion investigation in the hypersonic shock tunnel driver section," *Journal of Applied Physics* **30**, 1018–1021 (1959).
- ¹⁶⁸R. Stalker, R. Morgan, and A. Paull, "A shock tunnel investigation of scramjet performance with partially premixed combustion," in *Space Plane and Hypersonic Systems and Technology Conference* (American Institute of Aeronautics and Astronautics, 1996).
- ¹⁶⁹I. T. OSGERBY, H. K. SMITHSON, and D. A. WAGNER, "Supersonic combustion tests with a double-oblique-shock SCRAMjet ina shock tunnel," *AIAA Journal* **8**, 1703–1705 (1970).
- ¹⁷⁰E. N. Hoffman and C. S. Combs, "Design considerations and analysis of the utsa hypersonic ludwig tube facility," (AIAA Region IV Student Conference 2019, Austin Texas, USA, 2019).
- ¹⁷¹"Wind tunnels of nasa: Chapter 5 - the era of high-speed flight, coordination and cooperation: The national unitary plan," <https://history.nasa.gov/SP-440/ch5-12.htm>, accessed: 2021-10-15.
- ¹⁷²E. N. Hoffman, I. Bashor, and C. S. Combs, "Construction of a mach 7 ludwig tube at UTSA," (American Institute of Aeronautics and Astronautics, 2020).
- ¹⁷³S. Downes, A. Knott, and I. Robinson, "Towards a shock tube method for the dynamic calibration of pressure sensors," *Philos Trans A Math Phys Eng Sci* **372**, 20130299 (2014).
- ¹⁷⁴Q. Li, Z. Wang, Z. Wang, and H. Yan, "Novel method for estimating the dynamic characteristics of pressure sensor in shock tube calibration test," *Review of Scientific Instruments* **86**, 065002 (2015), <https://doi.org/10.1063/1.4921853>.
- ¹⁷⁵A. Arunkumar, Y. Srinivasa, G. Ravikumar, K. Shankaranarayana, K. Rao, and G. Jagadeesh, "A new shock wave assisted sandalwood oil extraction technique," in *Shock Waves* (Springer, 2005) pp. 1235–1239.
- ¹⁷⁶S. R. Nagaraja, J. K. Prasad, and G. Jagadeesh, "Theoretical–experimental study of shock wave-assisted metal forming process using a diaphragmless shock tube," *Proceedings of the Institution of Mechanical Engineers, Part G: Journal of Aerospace Engineering* **226**, 1534–1543 (2012), <https://doi.org/10.1177/0954410011424808>.
- ¹⁷⁷I. Obed Samuelraj and G. Jagadeesh, "Shock tubes: A tool to create explosions without using explosives," in *Blast Mitigation Strategies in Marine Composite and Sandwich Structures*, edited by S. Gopalakrishnan and Y. Rajapakse (Springer Singapore, Singapore, 2018) pp. 337–356.
- ¹⁷⁸S. S. Kubsad, B. Siddeswarappa, and B. Sridhar, "Effect of shock waves on wear behavior of few metallic materials," *Int. J. Eng. Sci. Technol* **4**, 2425–2431 (2012).
- ¹⁷⁹R. G. Morgan and R. J. Stalker, "Fast acting hydrogen valve," *Journal of Physics E: Scientific Instruments* **16**, 205–207 (1983).
- ¹⁸⁰S. O'Byrne, M. Doolan, S. R. Olsen, and A. F. P. Houwing, "Analysis of transient thermal choking processes in a model scramjet engine," *Journal of Propulsion and Power* **16**, 808–814 (2000), <https://doi.org/10.2514/2.5645>.
- ¹⁸¹A. Gardner A. D., Paull and M. T. J., "Upstream porthole injection in a 2-d scramjet model," *Shock Waves* **11**, 369–375 (2002).
- ¹⁸²A. M. Loske, "Medical and biomedical applications of shock waves," (2017), 10.1007/978-3-319-47570-7.
- ¹⁸³D. P. Gnanadhas, M. Elango, S. Janardhanraj, C. Srinandan, A. Datey, R. A. Strugnell, J. Gopalan, and D. Chakravorty, "Successful treatment of biofilm infections using shock waves combined with antibiotic therapy," *Scientific reports* **5**, 1–12 (2015).